Chem Soc Rev

RSC Publishing

REVIEW ARTICLE

View Article Online
View Journal | View Issue

Cite this: *Chem. Soc. Rev.*, 2013, **42**, 6840

Electronic structure of ions and molecules in solution: a view from modern soft X-ray spectroscopies

Kathrin M. Lange*[ab] and Emad F. Aziz*[bc]

Received 11th January 2013

DOI: 10.1039/c3cs00008g

www.rsc.org/csr

Soft X-ray spectroscopies are powerful tools for probing the local electronic and molecular orbital structures of materials in different phases and various environments. While modern spectroscopic tools using soft X-ray synchrotron photons perspicuously reveal the molecular orbital (MO) structure in detail, structures remain widely unknown in the liquid phase since many of these techniques could only be applied to solutions very recently. Furthermore, the interactions and dynamics of molecules in the liquid phase are especially complicated compared to those in gas and solid phases and thereby impede the understanding of functional materials in solution. This review presents recent developments using soft X-ray radiation for probing the electronic structure of ions and molecules in solution. The presented X-ray absorption, emission, and photo-electron spectroscopy studies exhibit the powerful contributions of soft X-ray liquid spectroscopies in the last few years.

1. Introduction

Quantum chemical calculations have improved our understanding of charge distributions in molecules[1] and the delocalization of electrons in bonds.[2] So far, it has been possible to obtain such information from theoretical calculations, *e.g.*, modern semi-empirical calculations *via* Mulliken population analysis.[3] The properties of the highest occupied molecular orbital (HOMO) and the lowest unoccupied molecular orbital (LUMO) play the main roles in many chemical reactions and determine electronic band gaps as well as manipulate charge transfer in complexes.[4] On one hand the energy of the HOMO is directly related to the ionization potential and describes how prone a molecule is to electrophilic attack. On the other hand, the energy of the LUMO is directly related to the electron affinity and is a measure for the susceptibility of the molecule and its affinity toward nucleophilic

[a] *Max Born Institute for Nonlinear Optics and Short Pulse Spectroscopy, Max-Born-Str. 2a, 12489 Berlin, Germany. E-mail: kathrin.lange@mbi-berlin.de*
[b] *Joint Ultrafast Dynamics Lab in Solutions and at Interfaces (JULiq), Helmholtz-Zentrum Berlin für Materialien und Energie, Albert-Einstein-Strasse 15, D-12489 Berlin, Germany. E-mail: Emad.Aziz@helmholtz-berlin.de, Kathrin.Lange@helmholtz-berlin.de*
[c] *Freie Universität Berlin, FB Physik, Arnimallee 14, D-14195 Berlin, Germany. E-mail: Emad.Aziz@fu-berlin.de*

Kathrin M. Lange

Dr Kathrin M. Lange did her PhD at HZB in the group of Prof. Aziz where she worked on setting up the LiXEdrom spectrometer and used it to study liquids and solutions. For her work she was awarded the Wilhelm-Ostwald-Nachwuchspreis 2012. As a postdoc she worked at the Max-Born Institut Berlin conducting ultrafast spectroscopy on liquids. Based on her Helmholtz-Postdoc Grant she is currently at HZB in the group of Prof. Aziz and as a guest scientist at the EPFL Lausanne in the group of Prof. Chergui, focussing on the investigation of the hydrogen bond network in liquid systems.

Emad F. Aziz

Prof. Dr Emad F. Aziz is a professor of physics at Freie Universität Berlin and the head of the Structure and Dynamics of Functional Materials in Solution department at Helmholtz-Zentrum Berlin. He is developing techniques to investigate liquids, solutes and interfaces with soft X-ray light sources. His work was honored with several prizes, most recently, the Karl-Scheel Preis 2011 and an ERC Starting Grant 2011. For more information, see: http://www.helmholtz-berlin.de/forschung/funkma/materialien-loesung/index_de.html, http://www.physik.fuberlin.de/en/einrichtungen/ag/ag-aziz/index.html.

attack. Accordingly the HOMO/LUMO orbitals are indicators for hard and soft nucleophiles and electrophiles.[5] Additionally, the HOMO–LUMO gap is an important stability index.[6] A large HOMO–LUMO gap implies high molecular stability in the sense of lower chemical reactivity.[7]

Soft X-ray spectroscopies allow us to study the properties of the HOMO and the LUMO and to obtain beyond this information about the other occupied and unoccupied molecular orbitals. Most chemical reactions take place in a liquid environment. In order to study these processes under realistic conditions with regard to, *e.g.*, pH, temperature, pressure, *etc.*, significant efforts have been made within the last few decades to make soft X-ray spectroscopies applicable to solution. In this review, the focus is on the spectroscopic methods based on soft X-ray photons with energies between 50 eV and 2000 eV obtained from high brilliant synchrotron light sources and their recent contributions to describe MOs in solution.

In the following section X-ray absorption spectroscopy (XAS), X-ray emission spectroscopy (XES) and resonant inelastic scattering (RIXS) are introduced as well as photoelectron spectroscopy (PES) and Auger electron spectroscopy. After that, the special challenge of investigating solution with soft X-rays is highlighted together with the recent technical approaches. The relation between probing the MOs and the chemical bond will be shown in various recent examples for each technique.

2. Soft X-ray spectroscopy

Modern optical spectroscopies have paved the way for describing the nature of HOMOs and LUMOs in detail for complicated biochemical systems. An interesting example is the CO binding process to the active center of myoglobin.[8–10] Lim *et al.*, *e.g.*, examined the orientation of bound CO to myoglobin by detaching CO from carboxy-myoglobin with polarized laser pulses followed by the investigation of its recombination to the active center by infra-red absorption.[10] Accordingly, detailed information for the binding of CO to the iron center of the myoglobin was acquired. In such absorption spectra, one can see all outer valence states, in this case including contributions from the iron, carbon, nitrogen and oxygen atoms. Nevertheless, it is of interest to explicitly and selectively see the MOs of the iron center during such a recombination process. For this purpose soft X-ray based spectroscopies can deliver atom specific electronic structure.[11–15] In the following the processes on which these methods are based are briefly explained. In Fig. 1 the basic processes of XAS, XES, PES and Auger electron spectroscopy are presented schematically. In the XA process a core–hole is created upon X-ray irradiation. The core–electron can be transferred to one of the unoccupied electronic states of the molecule or to the continuum. The transition probability of this process depends on the local density of states (DOS) and it obeys the dipole selection rules.[16] XAS accordingly allows probing the DOS of the unoccupied orbitals of a system as well as the symmetry properties of these orbitals. It has to be considered, however, that the presence of the core–hole modifies the DOS and therefore excited-state information is revealed. A detailed theoretical description of XAS can be found in the literature.[16]

While XAS allows deriving information about the nature of the unoccupied orbitals, PES reveals the occupied electronic structure.[17] The method is based on the photoelectric effect. Upon X-ray irradiation an electron from the core or outer molecular orbitals is emitted. The kinetic energy of an emitted electron is characteristic of its original electronic state. From the kinetic energy of the emitted electrons, the electron binding energies can be obtained as the difference between the excitation photon energy and the electron kinetic energy, neglecting the work function. Note that also PES does not probe the ground state binding energies, since the final state of the photoemission process affects the MOs. More details about PES can be found in the literature.[18]

XES and Auger spectroscopies are based on secondary processes.[17,19–21,92–96] When the core–hole created in the XA process is filled by an electron of smaller binding energy, the excess energy can be sent out *via* photons or electrons. This excess energy allows revealing information about the occupied molecular orbitals. For XES the photon energy of the emitted photons is of interest. These photon energies are characteristic of transitions, revealing information about the excited-state occupied electronic structure. As shown in Fig. 1, XES can be described as a two-step process, in which photon absorption and photon emission are considered as two decoupled processes. Accordingly, the transition probability to the final state is described by the product of the probability of the excitation to the intermediate state (the excitation process) and the probability for the relaxation to the final state (the emission process). This model is time independent so that it cannot reveal information about the dynamics of a system. It is valid when only one intermediate state exists. Upon approximating the process as a three-step mechanism, in which the intermediate state may undergo changes, conclusions about dynamics in the range of the core–hole lifetime are possible (core–hole clock).[22] When several intermediate states are accessible, the channels can interfere. In this case the process has to be treated as a one-step scattering process, called resonant inelastic X-ray scattering (RIXS), which is described by the Kramers–Heisenberg formula.[23,24] Within this scattering picture, effects of ultrafast dynamics of a system can be probed upon detuning from a resonance.[25] The theory of RIXS and its fundamental aspects can be found in detail in the literature.[22,24,26–30]

For Auger electron spectroscopy the kinetic energy of the emitted Auger electrons is of interest. When the core–hole is filled by an electron of an upper shell, the release of energy can lead to the emission of an electron. The kinetic energy of this Auger electron corresponds to the difference between the release-energy of the relaxation process and the ionisation energy of the Auger electron. Upon core-excitation of light elements with soft X-ray photons the emission of Auger electrons is the dominant process compared to emission of fluorescence photons. The high yield and the shallow escape depth of electrons from matter make electron detection the method of choice for surface or near-surface measurements.[31] The mean

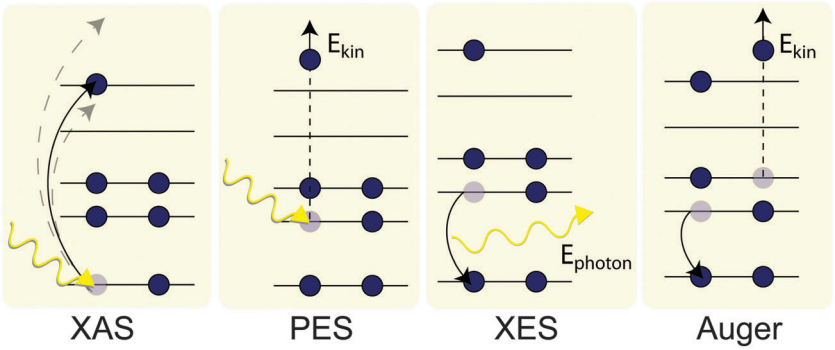

Fig. 1 Schematic of the X-ray absorption process (XAS), photoionization of an electron into the continuum (PES), spontaneous radiative decay of a valence electron into the core hole, known as spontaneous X-ray emission (XES) and emission of an Auger electron upon core hole relaxation (Auger).

free path of an electron with kinetic energy between 10–1000 eV is below 1 nm according to the universal curve in solids.[32] Yet, this limits feasibility to probe bulk properties with electron detection. Even though orders of magnitude less efficient, methods based on photon detection are usually chosen when the bulk structure of a sample is of interest.

Based on these spectroscopic methods detailed information about HOMO − n and LUMO + n on the surface and the bulk of the solution can be obtained, which determine the properties of the chemical bond of a system.

3. Investigation of solutions using soft X-ray photons

Energetically, soft X-rays are located in between extreme ultraviolet radiation (EUV) and hard X-rays. Since the soft X-ray photon energies match with atomic resonances and absorption edges of most low and intermediate Z elements (from $\sim Z = 5$, Z is the atomic number) soft X-ray spectroscopies offer great opportunities for both science and technology. Soft X-rays allow probing core to valance transitions through K-edges of the so called life-elements, *i.e.*, oxygen, nitrogen, and carbon, and the L-edges of 3d-transition metals. 3d-transition metals with their incompletely filled d-subshell are of special interest for the field of coordination chemistry, which is dedicated to the study of the interaction between transition metals with organic and inorganic ligands. Transition metals are able to adopt multiple oxidation states and many are highly efficient catalysts. They can be also found in the active centre of proteins *e.g.*, hemoglobin, myoglobin, or photosystem II, where they determine the function of the system. Understanding the electronic structure of transition metals in solution will serve as the first step towards understanding the more elaborate interaction, *e.g.*, between a transition metal and ligands within an active centre. The investigation of liquids and solutions with soft X-rays is, however, challenging. The incompatibility of the high vapor pressure of liquids and vacuum conditions required for soft X-ray measurements made such studies impossible for a long time. The development of several technical approaches allowed dealing with this problem.

a. Membrane-based techniques

Yang and Kirz used in 1987 two soft X-ray transparent Si_3N_4-windows to separate a thin water film from the vacuum surrounding.[33] For such membranes of, *e.g.*, 100 nm thicknesses, transmission for approximately 20% of the incoming photons is possible.[34] Radiation induced sample damage is however a crucial issue, leading to the development of flow-cells for fluorescence-based techniques, which allow a continuous refreshment of the sample during the measurements (see Fig. 2a).[35–41,42] Also for transmission mode measurements which require a sample thickness in the μm-regime, flow-cells exist which allow refreshment between every XA spectrum[34] or even between every XA measuring point[43] (see Fig. 2b). Recently Kolmakov *et al.* showed that with very thin graphene oxide windows photoelectron spectroscopy can be carried out as well.[44] However, even in flow-cells radiation damage may still occur due to a relatively slow flow speed. It also has to be considered that membranes are not ideally transparent in all energy ranges. Accordingly, absorption edges of elements that are contained in

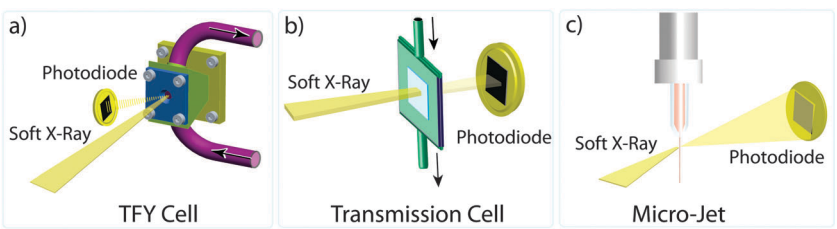

Fig. 2 (a) Schematic of a flow-cell for detection in fluorescence yield. (b) Schematic of a flow-cell for soft X-ray spectroscopy in transmission mode. (c) Schematic of a liquid micro-jet for fluorescence yield.

the membrane material cannot be investigated. Further, the sample could react with the membrane material and accordingly distort the experimental results. Membrane coatings, *e.g.*, Au coating, can protect the membrane from reacting with radicals created upon X-ray irradiation.[39]

b. Liquid-jet techniques

A different approach to bring liquids together with soft X-rays was shown by H. Siegbahn and K. Siegbahn who were the first to introduce the ''liquid beam'' technique to X-ray photoemission experiments on continuously fresh liquid samples.[45] With a jet-diameter of *ca.* 0.2 mm their approach was limited to the investigation of liquids with vapor pressures lower than 1 Torr.[45] Faubel and co-workers developed the idea further to the liquid micro-jet technique which allows obtaining stable vacuum conditions also for liquids with higher vapour pressure.[46] This was achieved by using a liquid jet diameter of, *e.g.*, only $\sim$20 μm produced in a glass nozzle and flow velocities between 30 and 120 m s^{-1} (see Fig. 2c).[46] In large parts the liquid from the micro-jet is detained from evaporating by freezing it inside a liquid nitrogen cooled container. Additional cryotraps and turbo-pumps are required to obtain the necessary vacuum conditions. Recently also techniques for recycling the solution from the micro-jet became available upon collecting the liquid after irradiation inside a differentially pumped container, which can be depleted from outside.[47] This is advantageous especially for expensive or rare samples; however, possible sample damage has to be considered then. Originally developed for methods based on electron detection, the liquid micro-jet technique is by now also used for photon-detection-based approaches.[48–50] However, effects of evaporative cooling have to be considered when using the jet-technique. The temperature dependence on the distance to the nozzle opening was experimentally shown, *e.g.*, for liquid water and methanol streams injected into a high vacuum by Wilson *et al.*[51]

4. X-ray absorption spectroscopy

X-ray absorption spectroscopy allows obtaining information about the unoccupied electronic structure of a system by scanning through the near-edge region of an element. That is why one refers to this technique also as NEXAFS, which stands for near edge X-ray absorption fine structure. The extended X-ray absorption fine structure (EXAFS), which refers to structural information revealed by a scattering of the emitted electrons on neighboring atoms, will not be discussed in this review. In 1975, Dehmer and Dill have proposed a quantitative calculation for the near edge structure of a molecule,[52] opening the door for understanding the experimental NEXAFS spectra and using it for investigating molecules, inorganic complexes, biological systems and distorted systems. Significant numbers of reviews have been presented, demonstrating the power of XAS probing the local electronic structure and dynamics of systems in gas and solid phases[53,54] as well as thin organic films.[55] Recently, the contribution of soft XAS to investigate the local structure around solvated molecules[56] and the perspective of this technique for revealing the structure and dynamics of metalloprotein active centers[57] were discussed.

Experimentally the absorption cross section of a sample can be obtained in the transmission mode which means by measuring the incoming light and that transmitted through a sample. Transmission mode measurements however require an energy dependent optimization of thickness and/or concentration for each sample. Indirect ways to determine the absorption cross section are to detect the electrons or photons that are emitted after electrons of lower binding energy fill the created core–hole, giving rise to the total electron yield (TEY) and the total fluorescence yield (TFY), respectively. To a limited extent[58,59] the TEY and the TFY can be considered as proportional to the absorption cross section for dilute and thin samples and are therefore often used for recording X-ray absorption spectra. It is important to note that in general the TFY can be affected by the saturation effect,[59,60] which is sample concentration-dependent.[56,60–62] A method to measure XAS free from this artefact is the recently proposed ''inverse partial fluorescence yield'' (iPFY).[63–65] For this method one uses the fact that the fluorescence of a lower-energy transition, which is not resonantly excited, is reduced upon scanning through the energy at an edge of interest. This reduction is inversely proportional to the absorption of the resonant excitation. Total yield is used as a term to distinguish from partial yield (PY) methods where electrons or photons are discriminated based on their energy as discussed with examples in the XAS section. Fluorescence-based methods, like TFY or PFY, can probe bulk properties and in addition can be used in magnetic or electric fields.

In the following several examples using TFY for probing MOs in solution are presented, ranging from simple ions to complex molecules. Complications concerning the interpretation of TFY and PFY spectra along with a possible solution by using the inverse partial fluorescence yield (iPFY) instead are discussed in the following section. Also, the dark-channel-fluorescence-yield (DCFY) is presented, a charge transfer process which further distorts TFY spectra but could allow identifying the MOs' hybridization strength.[66–70] Additionally, towards the end of the section, the state dependent partial fluorescence yield (SD-PFY) mode for XAS and its strength to deliver quantitative information about the nature of molecular orbitals in solution is presented.

a. Total fluorescence yield X-ray absorption studies

Despite the widespread occurrence of ionic solutions in nature and their high importance, *e.g.*, for active transport mechanisms in the body, the question of how ions are accommodated in a solvent network is still poorly understood on the molecular level. In the last few years soft X-ray spectroscopies significantly contributed to a better understanding as will be shown in the following examples based on TFY XA studies. In Fig. 3 TFY XA spectra of NaCl aqueous solution obtained from a flow-cell are shown.[62] Here the p-type MOs of Na^+ in water are probed upon exciting the 1s core electrons. The overall spectral shape is characterized by three peaks at 1072.8 eV (A), 1075 eV (B), and

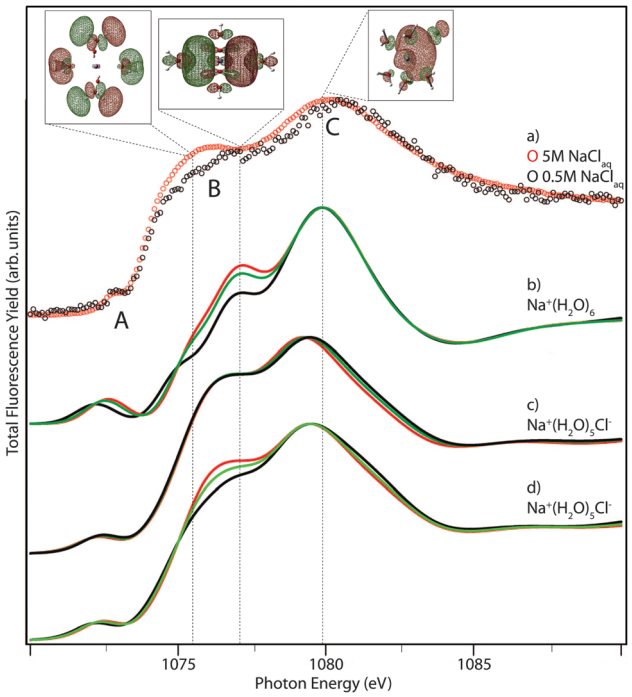

Fig. 3 (a) Sodium 1s TFY XAS spectra for 5 M and 0.5 M concentration of NaCl^{aq} solutions. (b) Calculated XA spectra for a Na$^+$(H$_2$O)$_6$ cluster for various Na–O distances (black: 2.37 Å, green: 2.35 Å, red: 2.30 Å). (c) Calculated XA spectra for a Na$^+$(H$_2$O)$_5$Cl$^-$ cluster with fixed Na–O distance of 2.4 Å and various Na–Cl distances (red: 3.5 Å, green: 3.6 Å, black: 3.7 Å). (d) Calculated XA spectra for a Na$^+$(H$_2$O)$_5$Cl$^-$cluster with fixed Na–Cl distance of 3.7 Å; and various Na–O distances (black: 2.35 Å, green: 2.38 Å, red: 2.4 Å red).[62]

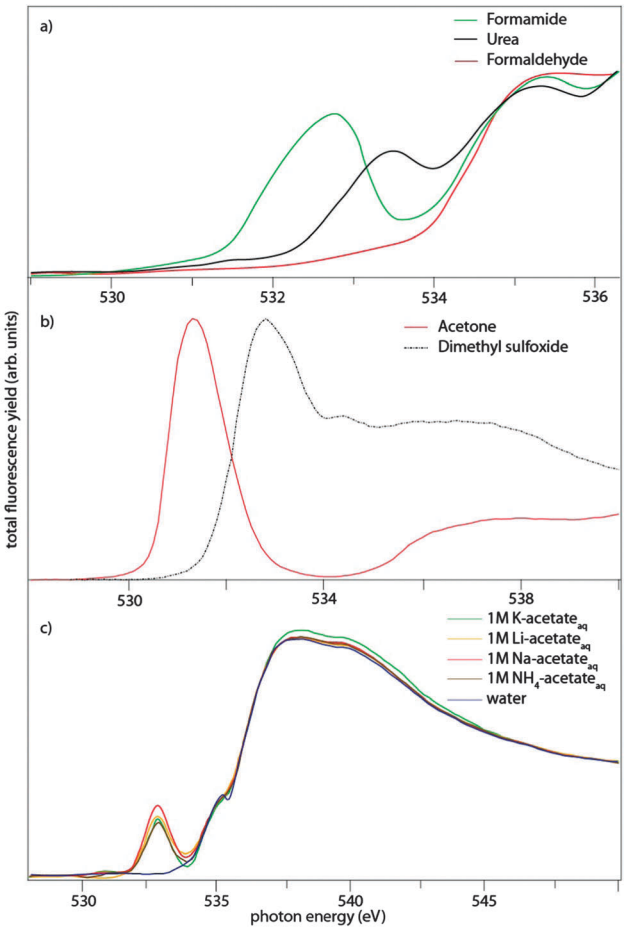

Fig. 4 Soft XAS at the oxygen 1s near-edge X-ray absorption spectra of; (a) urea, formamide and formaldehyde in aqueous solution,[73,74] (b) acetone and DMSO[14] and (c) different X–acetate (X = Li$^+$, Na$^+$, K$^+$, NH^{4+}) solutions.[79]

1080 eV (C). By varying the salt concentration the effect of the counter-ion on the Na$^+$ MOs can be studied. For lower concentrations the broad feature B splits up into two peaks. Using density functional theory the properties of the MOs under each feature can be revealed. From several high symmetry structures which were used to model the Na$^+$ environment best agreement was found for Na$^+$(H$_2$O)$_6$ and Na$^+$(H$_2$O)$_5$Cl$^-$ clusters. The respective calculated spectra are shown in Fig. 3. In the spectrum of the Na$^+$(H$_2$O)$_6$ configuration, the splitting of peak B can be reproduced. Systematic variation of the counter-ion distance in the Na$^+$(H$_2$O)$_5$Cl$^-$ cluster reveals an energy dependence of peak C, whereas changes in the Na–O distance lead to variations in the peak B intensity. Since one cannot cover all possible configurations in the calculations, it is important to consider that the study is qualitative. Based on such information about the MOs of Na$^+$ in aqueous solution, thermodynamic information could be obtained. For example, Lange *et al.* have presented a microscopic picture of sodium ions dissolved in water–alcohol mixed solvents, explaining the discrepancies between theories and experiments regarding the non-ideality in the free energy of solvation.[71] The water component plays a key role in stabilizing the solvation shell in mixed solvents, revealed by a selective photochemical process occurring only in pure alcohol solvents. Note that such photochemical observation was not considered in previous studies for sodium in alcohol and lead to inaccurate interpretation.[41] Another useful information based on the obtained detailed picture for MOs of Na$^+$ in solution is the formation of clusters incorporating Na$^+$, OH$^-$, and water molecules for 1 M salt concentration at high pH.[72] From the experimental data, one OH$^-$ interacts on average with at least 2.4 ± 0.6 Na$^+$ ions at pH 13. This finding is in agreement with the results from molecular dynamics simulations, namely that on average three sodium cations are found within a 6 Å sphere around an OH$^-$ ion and that one of them is forming a contact ion pair.[72]

Applications of TFY XA spectroscopy are not limited to ionic species in solution. Also from larger molecules in solutions information on the local electronic structure of a selected element can be obtained, *e.g.*, about the existence of a single or a double-bond.[14,73,74] An example is shown in Fig. 4a, where the hydrolysation of formaldehyde to methanediol in an aqueous environment is studied based on oxygen K-edge TFY XAS obtained from a flow cell.[73,74] The spectra of hydrolyzed formaldehyde were compared to the ones of the structurally similar urea and formamide, which are in contrast not hydrolyzed in aqueous solution. The spectra of formaldehyde, urea and formamide aqueous solutions exhibit two main features: the strongest at 535.0 eV in all spectra is the pre-edge of liquid water, whereas the low-energy features at excitation energy 533.4 eV

were identified as characteristic of transitions to the π* MO of the carbonyl group. The disappearance of the π* MO for formaldehyde has been mainly attributed to the hydrolysation of formaldehyde to methanediol and also to a minor fraction of smaller oligomers. In the hydrolysation process the double bond of the formaldehyde's C=O carbonyl group is broken upon addition of water, thereby forming a OH–C–OH diol group. A more localized carbonyl group leads to a shift of the π* MO to lower energy, as reflected in the formamide carbonyl group compared to the urea carbonyl group. As the carbonyl group becomes delocalized, the π* MO peak shifts to higher energies. This effect can be also observed clearly in oxygen K-edge XA spectra of acetone *versus* dimethyl sulfoxide (Fig. 4b).[14] In this figure, the XA spectrum of acetone is dominated by the transition of an electron from the oxygen 1s orbital to the LUMO at 531.3 eV. The LUMO has π* character and due to the attractive potential of the core hole, the O 1s → π* resonance appears below the ionization limit.[75] The spectral features are much broader than the gas phase spectrum.[76] From the interpretation of the gas-phase features by Hitchcock *et al.*,[76] the broad peak between 535 eV and 538 eV was assigned to unoccupied valence MOs of the oxygen p-character. The peak at the lowest energy in the DMSO spectrum is found at 532.8 eV. Following Sze *et al.*, this peak was assigned to a transition from the oxygen 1s orbital to the LUMO, which, also in DMSO primarily has π* character.[77] Indeed, the π* resonance is only observed for molecules which have π bonding.[16] Thus, already this observation suggests the sulfinyl group rather has a double (S=O) bond than a single ($S^+ \rightarrow O^-$) bond as proposed before.[78] The features at higher energy of DMSO are most likely due to transitions to MOs with local oxygen p-character. The peak at 534.2 eV is of low-lying σ* character in the relatively weak sulfur–oxygen bond. For molecules with a carbonyl group, the σ* resonance lies in the continuum above the ionization potential (IP) due to its relatively strong anti-bonding character.

The oxygen K-edge XA spectra of a series of 1 M X–acetate aqueous solutions (X = Li^+, Na^+, K^+, NH^{4+}) as well as of pure liquid water are presented in Fig. 4c. This figure demonstrates how species containing a carboxyl group are clearly distinguishable from water in XA spectra.[79] For excitation energies of above *ca.* 534 eV, the solutions' O 1s XA spectra are dominated by the characteristic water features. These are the pre-edge at 535 eV, the main-edge at 538 eV and the post-edge at 540 eV, respectively.[79] At excitation energies lower than the water pre-edge, a clearly separated peak appears at 532.8 eV with a constant width of 1.2 eV (FWHM) for all carboxylates. This peak is a spectral signature of the carboxyl group and arises from the promotion of an O 1s core-level electron to the LUMO of π* character. The intensities of this peak change considerably. It decreases in the sequence $Na^+ > Li^+ > K^+ > NH^{4+}$ and thus follows, with the exception of lithium, the Hofmeister series. Note that observations of ion-specific effects on proteins date back as early as 1888 when Hofmeister recognized that inorganic salts can be ranked by their ability to ''salt out'' egg white protein in aqueous solution. Changing the counter ion has an effect on the intra-molecular interactions and thereby on the local density of unoccupied states at the oxygen site of the carboxyl group. The observed intensity changes quantitatively correlate with the strength of ion pairing. Intensities of the acetate-specific O 1s absorption signal are proportional to the total number of empty states of MOs with p-character in the integration interval. Higher peak intensities result from electron withdrawal from the carboxyl group by the cation which is directly connected to an increased number of empty carboxyl MOs of p-character. Changes in the water hydrogen-bonding network induced by the acetate salts are identified as well, manifested by intensity variations in the main/post-edge region of the sodium and potassium acetate solution spectra. These changes have been attributed to strong perturbations of the electronic structure of water molecules within the anion hydration shell. A focus review about the contribution of X-ray spectroscopies to the interpretation of the water hydrogen bond is shown elsewhere.[19] It is worth mentioning that ion-selective interactions play an important role in many chemical, environmental, and biological processes occurring in aqueous solution. The cationic interaction with the protein's carboxylate groups is of special interest due to its effect on protein association and enzymatic activity.

Another interesting absorption edge in the range of soft X-rays is the L-edge of the 3d-TM in solution.[61,80] Soft X-ray spectroscopy is especially appropriate for investigating the structure of metal centers in proteins[12,13,57] because (a) of the intrinsic core–hole lifetime width (0.5 eV) of p orbitals results in sharper spectral features than optical spectroscopies, (b) $2p_{1/2,3/2} \rightarrow 3d$ transitions are dipole-allowed, since according to the dipole selection rules, an excited electron is promoted to a state with an azimuthal quantum number differing by $\Delta l = \pm 1$, yielding more intense and more structured spectra than the quadrupole-allowed transition to the d-type orbitals, (c) $L_{2,3}$-edge features are directly proportional to the amount of d-character of unoccupied valence orbitals of the metal which play the main roles in chemical reactions, and (d) ligand field multiplet calculations are well established tools to interpret L-edge spectra, delivering a detailed description of the oxidation state, charge transfer, and geometry of the excited atom.[32] Nevertheless, ligand field multiplet calculations have a significant drawback for systems including hydrogen bonding, strong hybridization, and molecular interactions. Indeed, L-edge *ab inito* calculations would help describing the MOs more quantitatively and realistically and recently promising studies for the L-edge spectra of transition metals were shown.[81–83] In Fig. 5 the L-edge TFY XA spectra of the iron in hemin and hemoglobin (Hb) in aqueous solution are presented obtained from a flow-cell.[12] The spectra were reproduced with theoretical ligand field multiplet calculations.[12] The L_3 edges of the Hb and hemin in solution exhibit two main peaks at the same energies. While the first peak at 708.8 eV reveals slightly higher intensity for Hb compared to hemin, the second peak at 710.9 eV exhibits broadening on the low energy side for Hb. The L_2 edge of Hb exhibits a pre-edge peak at approximately 720.3 eV followed by two peaks at 722.2 eV and 724 eV, which lie 300 meV and 500 meV lower energetically than those for hemin, respectively. Theoretical modeling of the spectra[84] give quantitative

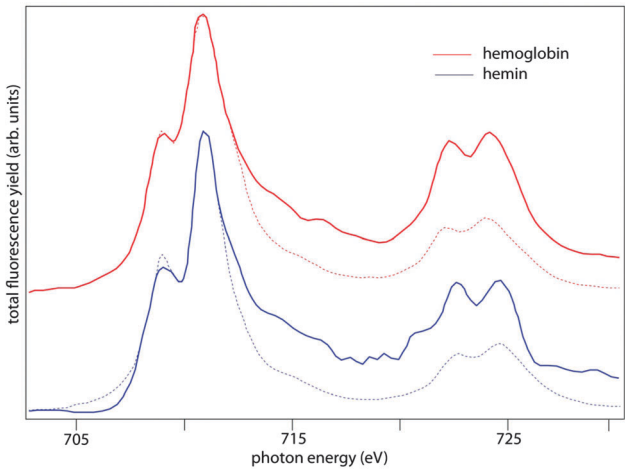

Fig. 5 Experimental Fe $L_{2,3}$ edge XA spectra of hemoglobin and hemin in solution (3 mM) recorded. The dotted lines represent the simulated Fe $L_{2,3}$ edge spectra calculated using the ligand field multiplet (LMF) theory.[12] Reprinted figure with permission from Aziz *et al.*, *Phys. Rev. Lett.*, 2009, **102**, 068103. Copyright 2009 by the American Physical Society.

information about bonding, back bonding, charge transfer, and spin character. It shows evidence that Hb and hemin in solution are in the high spin state. Presumably, this is due to the fact that no strong forces are exerted by the coaxial ligand on the Fe^{3+} center, as is the case in solid samples, which favor the low spin state. Upon dissolving the iron–porphyrin group in solution, it switches to the HS state causing the L-edge to exhibit high sensitivity to the coaxial ligand. Information about the strength of the σ and π bonds around the iron centre is obtained. An interesting conclusion is that the imidazole ligand in Hb and the chloride anion in hemin give a similar contribution to the σ-donation. Furthermore, the π-donation of the single imidazole ring to the metal in Hb is lower than what is observed in LS heme compounds connected with two imidazoles.[12,85] This suggests that imidazole is not only acting as a strong σ-donor but also a strong π-donor. In particular, the metal MO of Fe^{3+} increases compared with non-heme complexes due to the increased σ and π-donation from the porphyrin ring to the Fe^{3+} centre. Furthermore, a substantial π-back-donation from both, the porphyrin and the axial ligand, is observed. Note that the axial ligand in hemin is Cl^- on the one side and water on the other, while for Hb a proximal histidine is found on one side and water on the other.

Just very recently, L-edge XAS was used to investigate the nature of the interaction of different ligands with the porphyrin active centre of myoglobin in solution based on TFY-XAS.[86] Myoglobin is responsible for the storage and the transport of oxygen in muscle cells and ligands like O_2, CO, NO or CN can bind reversibly to its active centre. Iron L-edge X-ray absorption spectra of the active centre of myoglobin in the met-form, in the reduced form and upon ligation to O_2, CO, NO and CN revealed the ligation strength for each ligand, finger-printed through the variation of the $L_3 : L_2$ intensity ratio. Based on experimental observation, the strength of the interaction between the ligand and the porphyrin active centre is sorted in the following order: CN ≈ CO > O2 ≈ NO.

As mentioned before fluorescence yield measurements of the absorption coefficient can introduce artifacts which are connected to saturation effects in the detection technique; this is in particular the case for non-dilute, thick specimens.[59] The size of these distortions depends on the different contributions of the various atomic species to the X-ray absorption cross-section as well as on the overall geometry. But also for diluted samples, for which saturation should be negligible, further effects can distort the proportionality between fluorescence intensity and absorption cross section, as will be discussed in the following.

I. Distortion effects for TFY XAS and dark-channel-fluorescence-yield. The appearance of dips in the absorption spectra of L-edges of 3d-transition metal ions in aqueous solutions in TFY mode recently initiated the discussion about effects that can distort the proportionality between the fluorescence intensity and the absorption cross section.[66,67,70,87,88] Fig. 6 shows the $L_{3,2}$ TFY spectrum of Fe^{3+} ions in methanol and ethanol in comparison with the spectrum in water at a similar concentration.[66] For the aqueous solution some bands dip below the background level and truncate the main peak. In this case, obviously, one cannot consider the fluorescence signal obtained to be proportional to the absorption cross section of the iron. In this section effects like saturation, the influence of the background and non-radiative relaxation processes that have to be considered in this context will be discussed.

As mentioned above, for concentrated bulk samples saturation effects have to be taken into account.[59] The distortions due to saturation effects lead to an overemphasizing of low intensity spectral features with respect to high intensity ones. This effect depends on the geometry of the experiment. For grazing-incidence and normal-takeoff geometry, *e.g.*, maximal distortions are expected, since all photons are absorbed close to the surface of the sample. Due to the short way out of the sample, almost all fluorescence photons emitted in the direction of the

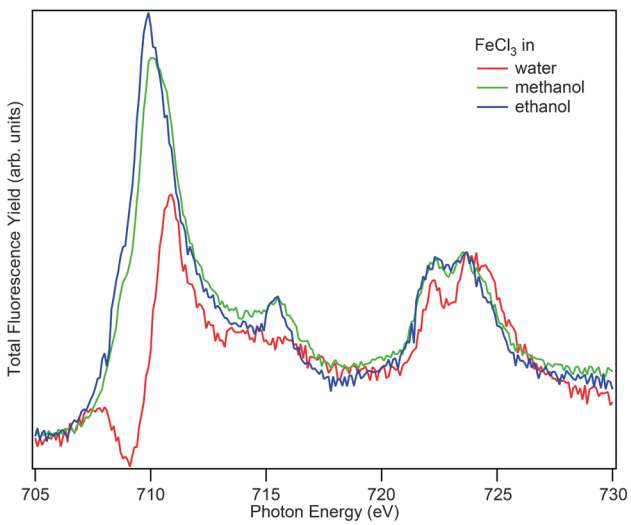

Fig. 6 Fluorescence-yield spectra in the $L_{2,3}$-edge region of Fe^{3+} ions in water *versus* ethanol.[66]

detector can reach the detector. Accordingly, the energy dependent fluorescence signal loses its proportionality to the absorption cross section.[59] Correction procedures for saturation effects are based, *e.g.*, on angle- or concentration dependent studies.[59,60]

Especially for TFY spectra of TM ions in aqueous solution the contribution of background signal has to be taken into account. The absorption L-edge of iron, *e.g.*, lies with ~707 eV energetically above the absorption edge of the oxygen of water (at 535 eV). Thus, when scanning across the iron L-edge, the oxygen of the water is concurrently excited. An increase of absorption by the iron leads to a decrease of the number of photons available for exciting the oxygen. The fluorescence background signal of the oxygen that should be approximately constant in the region of 700 eV would accordingly decrease upon scanning across the iron edge. The iron L_3-edge yield is slightly below the oxygen K-edge yield of water, so the fluorescence of the absorbing iron ions has a lower yield than that of the surrounding oxygen atoms and, accordingly, a dip can occur in the spectrum. This is less likely at the L_2 edge because its fluorescence contribution is higher. This effect was considered to be one contribution to the observation shown in Fig. 6.

As a second contribution a charge transfer from the metal d-orbital to the solvent was proposed that quenches the X-ray fluorescence from these states.[66] This so called dark channel fluorescence yield (DCFY) could allow determining the nature, directionality and the timescale of this electron transfer. It was proposed that the feature at 707 eV (Fig. 6) correlates with the first pre-edge feature of the oxygen K-edge spectrum of Fe^{3+}-containing aqueous solutions reported by Näslund *et al.*[2] The gradual prominence of sub-background features on dilution of $FeCl_3$ in water can be correlated to the increase in metal-to-ligand-charge-transfer (MLCT) from the iron orbitals. Such MLCT becomes stronger with the increase of MOs hybridization between the metal MOs (Fe^{3+} in this case) and the ligand MOs (water in this case). Observing such dips for Fe^{3+} in water and not in alcohol indicates a strong MOs hybridization of Fe^{3+} with water compared to alcohol. Such behavior is not limited to aqueous environments and the observation of sub-background features in fluorescence-yield spectra represents a novel and relatively simple method to identify the interaction of solutes with their environment in solutions and in heterogeneous media, such as interfaces, and to determine the direction of the electron transfer. This requires, however, to discriminate the DCFY from the distortion effects mentioned before.

The DCFY is currently still under investigation and initiated controversial discussions among scientists.[70,87,88] Based on pure theoretical simulation, *e.g.*, de Groot argued that the origin of the dips in the TFY spectra is state dependent decay, where lower spin states at the L-edge decay with less probability than the high spin states, causing the dips.[87] These calculations however did not include charge transfer effects. As mentioned earlier in this review, L-edge simulations need to go well beyond an atomic treatment, *i.e.*, beyond what is presented in de Groot's proposal,[87] and even beyond a parameterized charge-transfer description. Simulations need to take electronic-structure interactions between solute (ion) and solvent (water) into account, as was done, *e.g.*, by Näslund and coworkers.[2] It was shown recently by Seidel *et al.*, using the same multiplet program, that including charge transfer would give a simulated spectrum in well agreement with the experimental one.[68] Including charge transfer effects causes mixing of the spin states such that the spin states are not any more distinguishable. Accordingly, an argumentation based on a pure spin-state picture as proposed by de Groot is not realistic. Regier *et al.*[88] emphasize that the analysis of TFY spectra from transition-metal aqueous solution is complicated owing to competing signal contributions from solute and solvent, as described above in this section. They proposed the inverse partial fluorescence yield (iPFY) method,[88,89] which is considered to be a bulk sensitive method, delivering an X-ray absorption spectrum free from artifacts such as saturation/self-absorption effects. This technique will be discussed in detail in the following section with recent examples for liquid investigations. However, the sole use of iPFY does not allow a distinct conclusion concerning the existence of the charge delocalization channel. Further insight was gained by probing the non-radiative Auger-type electron emission channel using photoelectron spectroscopy (further details will be shown in the X-ray photoelectron spectroscopy section). The measurements unequivocally demonstrate that metal-to-water charge transfer quenches fluorescence which leads to a dip in the total-fluorescence-yield X-ray absorption spectrum. Energy resolved fluorescence detection techniques, like the PFY, iPFY and SD-PFY allow obtaining additional information and will be discussed with recent examples in the following section.

b. Partial and inverse partial fluorescence yield

For thin or dilute samples like in the previously presented iron L-edge XAS of hemoglobin (Fig. 5), where the concentration was in the order of few mM, saturation effects are negligible. For thick or high concentrated samples a method free from the artifacts in TFY was recently proposed by Achkar *et al.*[89] In what they termed "inverse partial fluorescence yield" (iPFY), one uses the fact that the fluorescence of a lower-energy transition, which is not resonantly excited, is reduced, and the reduction is inversely proportional to the absorption of the resonant excitation. The iPFY approach requires the presence of an observer element in the sample, which has an energetically lower lying absorption edge than the element of interest so that it is non-resonantly excited throughout the investigated energy range. For aqueous Fe^{2+}, the oxygen K-edge of water is a suitable observer, as its strong fluorescence is readily measured. Variations in the absorption strength of the sample while scanning the iron L-edge alter the number of photons available for the absorption by oxygen, in turn altering the oxygen fluorescence. Accordingly, the oxygen fluorescence is reduced when the iron L-edge absorbs stronger and *vice versa*. (see Fig. 7a) Inverting the oxygen fluorescence then allows a measurement of the L-edge's absorption strength. The first application of the iPFY method on a liquid sample was recently shown by Gotz *et al.* for aqueous Fe^{2+}.[90] For this experiment a high resolution X-ray emission spectrometer based on a Rowland circle design was used,[48,91] which is schematically presented in Fig. 7a. PFY spectra were obtained by integrating over the appropriate

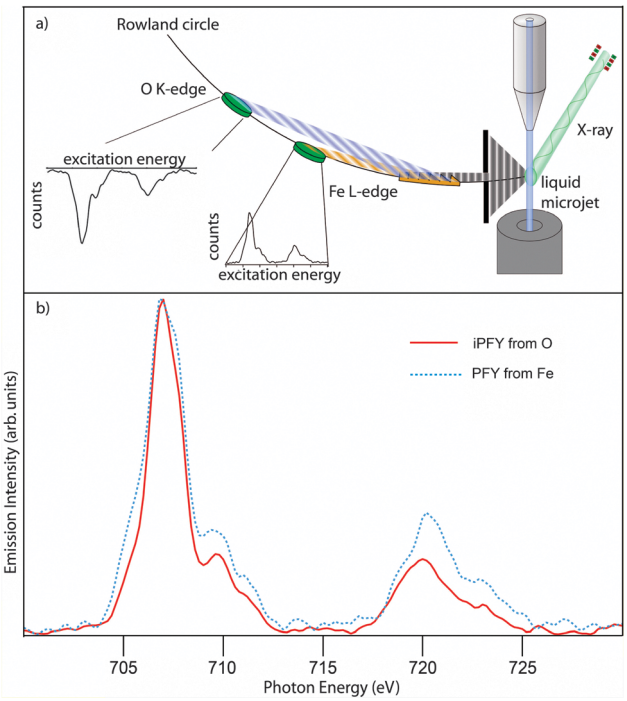

Fig. 7 (a) Inverse partial fluorescence yield (iPFY): measuring *e.g.* the iron absorption strength in an aqueous ionic solution *via* the reduction of the observer intensity (in this case oxygen). For separating the different photon energies, an XES spectrometer in Rowland-circle design can be used. The different detector positions for first-order oxygen and iron emission are sketched with the resulting spectra, upon scanning excitation energy. (b) Iron L-edge XAS of 1 M $FeCl_2$ solution in water using iPFY (the inverse of the oxygen emission) and the iron PFY spectrum.[90]

energy interval of the emission spectrum while varying the excitation energy. The oxygen PFY spectrum was inverted (iPFY) and compared to the iron PFY spectrum (see Fig. 7b). This allows drawing conclusions on Coster–Kronig (CK) transitions. In a simple picture, the significant L_3–$M_{4,5}$ emission at the L_2 resonance shows the presence of L_3 holes, which cannot stem from non-resonant excitation. This emission is a result of L_2–$L_3M_{4,5}$ Coster–Kronig (CK) decay following the creation of an L_2-core–hole. The CK transition is not possible in free atoms and becomes possible in metal through relaxation effects. Moreover, the rate is very sensitive to the outgoing electron's kinetic energy for low kinetic energies, which should be the case for a transition close to threshold. It is astonishing that the CK transition in doubly charged Fe^{2+} ions in solution is about as strong as in the Fe metal. This is indicative of strong interaction of the valance MOs of the Fe^{2+} with the water giving rise to significant screening effects. The effect appears to be strong enough to reduce the binding energies to levels comparable to uncharged solid states because the CK transition rates are so similar. The use of CK transitions is envisioned as a probe for the interaction of dissolved ions with their environment, also being connected to the electron dynamics at the solute–solvent interface. Probing the influence of varying ligands or solvents on the CK rate should allow insights into the strength of the chemical bond and ion–solvent interaction.

c. State dependent partial fluorescence yield

According to the previous section, the use of iPFY allows obtaining spectra free from saturation effects, but it does not allow investigating or quantifying the non-radiative decay at the L-edge of TM. Resolving this issue could be realized by discriminating between the various fluorescence contributions, in particular that of oxygen K_α from those of the metal L-edges and between the different L-edge contributions themselves. Such a method was recently developed and combined with the liquid micro-jet technique and named state dependent partial fluorescence yield (SD-PFY), which is schematically presented in Fig. 8a.[69] The results obtained by using this technique provide further evidence for the proposed DCFY

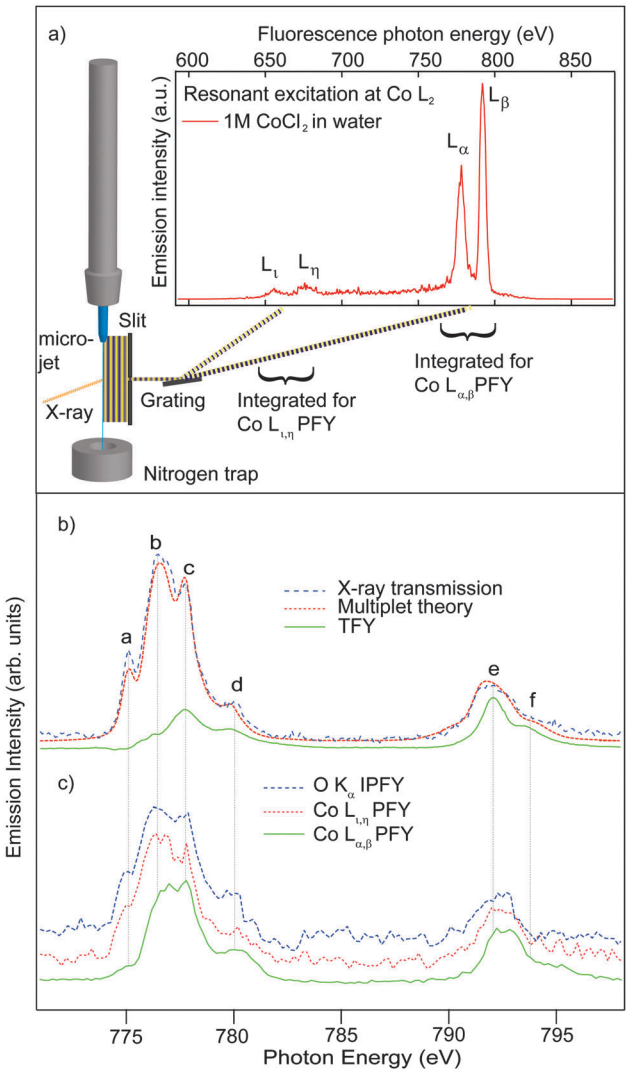

Fig. 8 (a) State dependent partial fluorescence yield (SD-PFY): contributions from different transitions are separately integrated in order to obtain FY spectra from specific states. For separating the different photon energies, an XES spectrometer in Rowland-circle design can be used. (b) Co^{2+} L-edge transmission, simulated and experimental TFY XA spectra of a 1 M aqueous solution of $CoCl_2$ at pH 5.9, obtained with 0.5 eV resolution. (c) L-Edge XAS SD-PFY–$L_{\alpha,\beta}$ and 3s $L_{\iota,\eta}$ of Co^{2+} in comparison with the iPFY–K_α.[69]

mechanism and go beyond the initial publication.[66] For this study a Co^{2+} aqueous solution was chosen as a sample system for the reasons that (a) recent photoelectron spectroscopy studies on this system combined with X-ray absorption and multiplet simulations have provided further support[68] in favor of the electron transfer to the solvent as a non-radiative channel[66] and (b) it is well established that in aqueous solution, Co^{2+} forms aqueo-complexes with water molecules coordinating to the metal.[92] The SD-PFY spectra are obtained by tuning the fluorescence spectrometer to individual lines of the emission spectrum while scanning across the $L_{2,3}$ absorption edges of Co^{2+} (Fig. 8a). The radiative decay channels that can possibly contribute to the TFY upon excitation of the Co 2p-orbitals are the $L_l(3s \rightarrow 2p_{3/2})$, $L_\eta(3s \rightarrow 2p_{1/2})$, $L_\alpha(3d \rightarrow 2p_{3/2})$ and $L_\beta(3d \rightarrow 2p_{1/2})$, in addition to the O K_α emission. The TFY and the transmission spectra compared to the state dependent partial yield spectra from the liquid micro-jet are shown in Fig. 8b and c. The XA spectrum measured in transmission mode (Fig. 8b) reflects the true absorption cross section and is thereafter used as a reference. A detailed discussion of this spectrum and its comparison with the partial electron yield spectrum is found in ref. 68. The O K_α iPFY spectrum is measured while the incident energy is scanned in the region of the Co L-edges. Since absorption by the Co L-edges does not feed the O K_α emission, the Co L-edge absorption spectrum appears below the base line. The inverse of this spectrum (Fig. 8c) is in good agreement with the transmission spectrum (Fig. 8b). The Co $L_{l,\eta}$ PFY XA spectrum is also in good agreement with the transmission spectrum after normalization. As this spectrum depends on the relaxation of a 3s-electron to the 2p core–hole, it would present the ''undisturbed relaxation''. In other words, electrons in the Co 3s orbitals relax to a core–hole giving unquenched photon-out events. The Co $L_{\alpha,\beta}$ PFY spectrum is less noisy than the Co $L_{l,\eta}$ PFY and the O K_α iPFY spectra because the $L_{\alpha,\beta}$ emission lines are more intense. By normalizing the iPFY spectrum at the L_2 edge, one can see that in contrast to the Co $L_{l,\eta}$ PFY spectrum and the transmission spectrum, band (a) is now reduced in intensity relative to the other features of the spectrum. This has been attributed to a quenching of the fluorescence due to non-radiative channels, such as electron transfer to the solvent. This is supported by the previous partial-electron-yield (PEY) XAS study, in which band (a) was also reduced relative to the transmission spectrum, due to the same mechanism.[68] This is reflected by the fact that the high-energy peaks are more radiative in the TFY. The reduction of the first peak in the Co^{2+} $L_{\alpha,\beta}$ PFY explains the total disappearance of this peak in the TFY, as the latter is also affected by the oxygen background.

In conclusion, the distortion of the L_3 *versus* the L_2 of TFY is due to (a) a charge transfer from the metal d-orbitals to the solvent which quenches the X-ray fluorescence from these states. In the case of Co^{2+} aqueous solution it reduces the intensity of the first peak in the TFY. (b) It is due to the competition between the fluorescence yields of the solvent species (*i.e.*, oxygen) *versus* that of the solute. This causes total disappearance of the first peak at the L_3 TFY of Co^{2+}, furthermore, reducing the intensity of the L_3 *versus* L_2 in the TFY spectrum.[70]

5. X-ray emission spectroscopy

In 1977, K. Siegbahn and his student J. Nordgren presented the first high resolution X-ray emission spectrometer,[93] and since this time the method has been used and developed further for a wide range of applications. In the last two decades the development of instrumentation[94–96] for X-ray emission (XES) and its resonant process, resonant inelastic X-ray scattering (RIXS), has established these methods as suitable tools for probing localization of valence electrons in the atom specific picture.[97–101] Their application to liquids combined with the use of soft X-ray photons has been discussed in recent reviews.[19,20] One of the strong motivations for scientists to challenge emission spectroscopy in liquid is, *e.g.*, to understand the hydrogen bond network of water.[19,102] Detailed information about the contribution of RIXS and XES for describing waters' hydrogen bond network is presented in a recent review.[19]

Combining XES and RIXS with soft X-ray photons allows interesting insights into the electronic structure dynamics of the occupied MOs in solution. The first example here will be the investigation of acetone and DMSO, whose unoccupied MOs were already discussed in the X-ray absorption section.[14] Fig. 9 shows the RIXS and XE spectra of acetone and DMSO. The RIXS spectra of acetone excited on the oxygen $1s^{-1}\pi^*$ resonance and the non-resonantly excited XE spectra are presented in Fig. 9a.[14] Note that in the RIXS process also the excited electron can fill the core–hole in transitions to the electronic ground state, giving rise to a quasi-elastic line with energy losses due to vibrations. The highest energy feature corresponds to the elastic scattering and can be used for energy calibration. Apart from this feature, there are unresolved vibrational progressions,[103] which are dominantly due to the C–O stretching mode. Such unresolved vibrational modes are discussed by Sun *et al.* demonstrating a unique sensitivity of the method to the local potential energy surface in complex molecular systems.[103] The resolved spectrum is shown in Fig. 9b. The authors used simulations which are based on *ab initio* calculations of dipole moments and potential energy scans for all vibrational modes in the acetone molecule. According to the theoretical analysis only eight modes are active: CO stretching, CCC deformation, CO out-of-plane bending, CCS stretching, CH_3 rock, CH_3 s-deformation, and two torsion modes due to two CH_3 rotors. Fig. 10 presents a combination of the XAS with the RIXS potential energy curve (Fig. 10a), explaining the absorption and emission spectra (Fig. 10b and c, respectively). To understand the remaining emission peaks of acetone, one uses the description of the Zheng *et al.*,[104] for the occupied orbitals for a single acetone molecule with the C_{2v} symmetry in the increasing energy order which is: $1a_1$, $2a_1$, $1b_2$, $3a_1$, $4a_1$, $5a_1$, $2b_2$, $6a_1$, $3b_2$, $7a_1$, $1b_1$, $1a_2$, $8a_1$, $4b_2$, $2b_1$, and $5b_2$ (HOMO). Labeling the emission peaks based on these molecular orbitals is shown in Fig. 9.

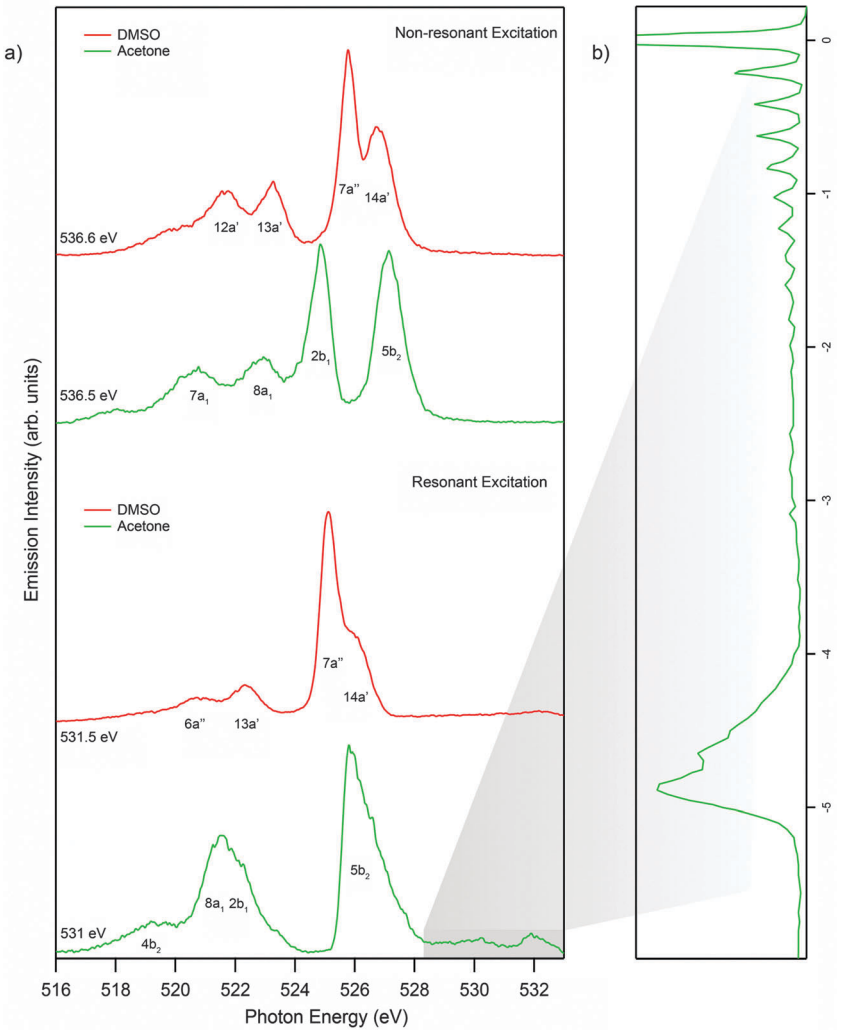

Fig. 9 (a) Non-resonant (XES top) and resonant emission (RIXS bottom) spectra of acetone and DMSO measured along the oxygen K-edge excitation. The excitation energies are indicated on the left side of each spectrum.[14] (b) Zoom out of the unresolved vibronic state in the emission spectrum, which is resolved by Sun *et al.*[103] using high resolution RIXS. Reprinted Fig. 9b with permission from: Y.-P. Sun *et al.*, *Phys. Rev. B*, 2011, **84**, 132202, Copyright 2011 by the American Physical Society.

The RIXS and XE spectra of DMSO show different trends compared to the ones of acetone. The elastic scattering peaks (at 532 eV) are less prominent for DMSO than for acetone. This indicates that the excited electron is less localized in DMSO than the electron in the $1s^{-1}\pi^*$ excitation in acetone. Another distinction is the shift of the valence peaks towards higher energies as the excitation energy increases within the first resonance (for clarity see ref. 14). For higher energy excitation, beyond the first resonance, the valence peaks do not show any energy shift or change in the relative structure. DMSO has a lower symmetry (Cs symmetry) compared to acetone. According to the theoretical analysis of the MOs, the occupied orbitals for a single molecule are: 1a′, 2a′, 1a″, 3a′, 4a′, 5a′, 2a″, 6a′, 7a′, 8a′, 3a″, 9a′, 10a′, 4a″, 11a′, 5a″, 12a′, 6a″, 13a′, 7a″, and 14a′ as the HOMO. 15a′ and 8a″ are the close-lying LUMO and LUMO + 1, respectively.

It has been shown by Atak *et al.*[14] that stretching DMSOs energy scale leads to a good agreement with the acetone spectra. This may be surprising considering the large difference between the molecules. As the spectra reflect the local electronic structure at the oxygen site, this result suggests that the oxygen atom interacts in a similar way with neighboring atoms in DMSO and acetone. The spacing between the peaks is directly related to the spacing between the final states. In the MO picture, the wider spacing between the valence orbitals in acetone is interpreted as a larger overlap between the atomic orbitals than the corresponding overlap in DMSO. The difference in overlap in the bonding molecular orbitals can be directly associated with the difference in strength of the C–O and S–O bonds of the two molecules. Besides the energy spacing, the largest difference between the two spectra concerns the two peaks at the highest energy (see non resonant excitation spectra in Fig. 9). In both spectra the highest-energy peak can be assigned to final states with a vacancy in the HOMOs. The difference between the two spectra is that the intensity in the DMSO spectrum is about half the corresponding

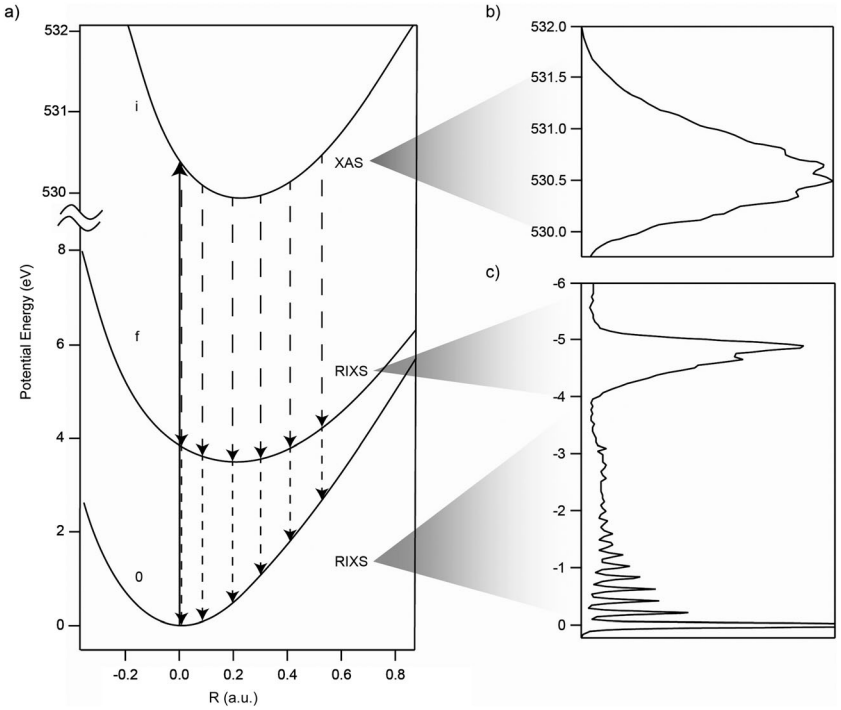

Fig. 10 (a) The formation of the RIXS spectrum is illustrated for the CO stretching mode. (b) The absorption spectrum at π* shown in the upper right corner and the RIXS spectrum. (c) The RIXS spectrum at π* resonant excitation.[103]

intensity in the acetone spectrum.[14] This indicates that the HOMO in DMSO has less oxygen p-character compared to the HOMO in acetone. In both molecules these orbitals are often termed oxygen ''lone-pair'' orbitals, and the present results indicate that the lone-pair character of the HOMO is much less pronounced in DMSO. The second peak corresponding to final states with a vacancy in HOMO−1 shows a strong additional energy shift when comparing acetone and DMSO spectra. In acetone, the HOMO−1 orbital is π-bonding, with coinciding nodal and molecular planes. In DMSO the HOMO−1 orbital has also the π-bonding character but the situation is complicated in the molecular geometry where the S–O bond is bent out of the molecular plane, and the anti-bonding interaction with the methyl groups is more prominent than for acetone. The π-bonding due to the HOMO−1 in acetone is thus much weaker in DMSO, reflected by the additional energy difference between the corresponding peaks.

It is well known that DMSO has a large dipole moment with excess negative charge at the oxygen site. Comparing acetone and DMSO, there is, however, a small redistribution of intensity from the ''lone pair'' peak to the low-energy part of the spectra, which according to theoretical calculations corresponds to the $6a_1$ orbital in acetone (see Fig. 9). This increased relative XE intensity in the DMSO spectrum suggests a polarization towards the oxygen atom, thus weakening the S–O bond further. Accordingly, the partially charged oxygen in the sulfinyl group originates from the deeper valence orbitals rather than from the highest ones. This leads to a higher dipole moment for DMSO compared to acetone. Furthermore, as the partial charges originate from the deeper valence orbitals, DMSO interacts mainly electrostatically with the neighboring molecules.

Another issue that was discussed by Atak *et al.*[14] is the difference in the HOMO–LUMO energy gap between acetone and DMSO. While it is of 4.2 eV in acetone, in DMSO it is of 6 eV. Interestingly, the ratio of the dipole moments for DMSO and acetone is 1.4, which is equal to the energy gap ratio. As mentioned in the Introduction of this review the HOMO–LUMO gap is an important stability index for a molecule.[1] A large HOMO–LUMO gap implies high stability, which reflects low reactivity toward chemical reactions. Furthermore, according to Pearson, the increase of the HOMO–LUMO gap increases the hardness of the molecule.[105] Since hardness is also related to nucleophilicity and electrophilicity, this indicates that DMSO is more nucleophilic and electrophilic than acetone.

Physical properties like the freezing point of samples can vary significantly when their environment is changed. When mixing DMSO with water, *e.g.*, the freezing point is depressed by 140 K at molar fraction of *x*DMSO = 0.25 to 0.3. The effects that go along on the molecular scale with such physical changes can be studied using XES and RIXS. Upon mixing DMSO and water and comparing the spectra to a superposition of the spectra from the pure liquids, the deviations indicate strong interactions between the molecules.[106] The spectral changes are associated with rearrangements of HB conformations, as will be briefly discussed in the following. To the non-resonantly excited XE spectra shown in Fig. 11a oxygen atoms from both molecules, DMSO and water, contribute. In solutions with large water content (DMSO is <50 vol%) it is expected that the spectra are dominated by emission from water, and features

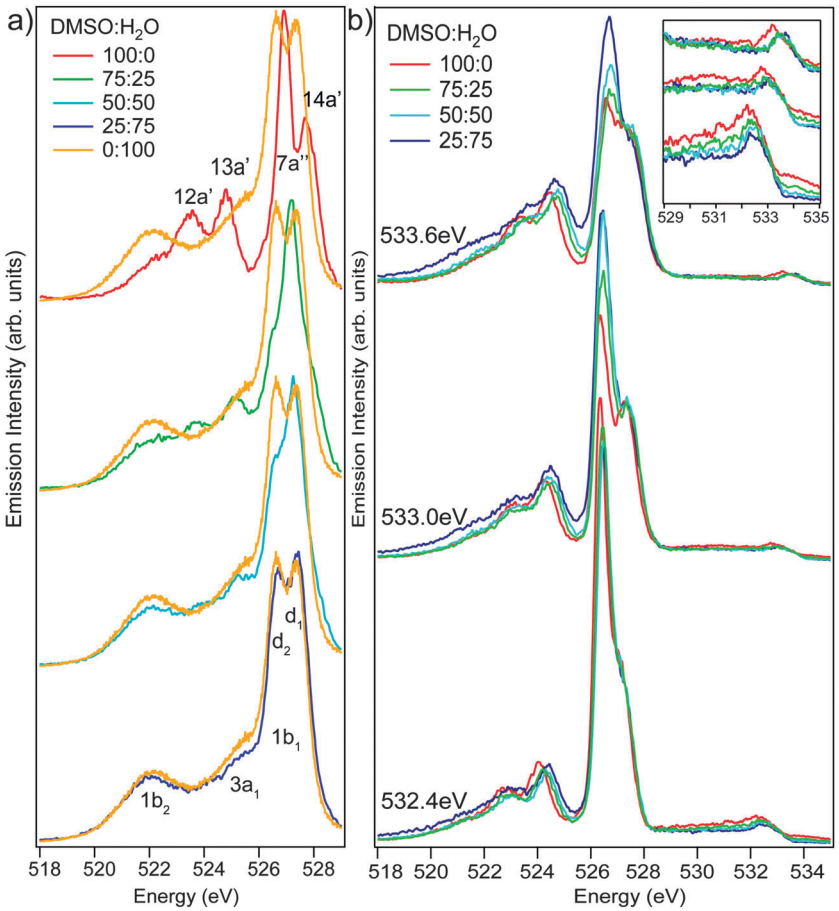

Fig. 11 (a) Non-resonantly excited (537.7 eV) XE spectra of pure DMSO (red), DMSO–water mixtures with 75 : 25 (green), 50 : 50 (light blue), 25 : 75 (dark blue), and pure water (yellow). (b) RIXS spectra of pure DMSO and its mixtures with water with volume ratios 25 : 75, 50 : 50, and 75 : 25. The respective excitation energies are shown above the spectra. The elastic peaks are presented separately in the inset for better visibility.[106]

reminiscent of DMSO are not very prominent. An obvious difference from the spectrum of neat water is, however, the relative reduction of the lower intensity features of $1b_1$ MO intensity. In line with earlier results[91,107] this observation is interpreted as a "fingerprint" for breaking of HBs in the water network when DMSO molecules are introduced. A noticeable effect is observed already at 25 vol%, and at 50% concentration the reduction is comparable to dissolution of water in 25% acetonitrile.[91] Since the HBs between DMSO and water at the DMSO oxygen site are much stronger than typical HBs in the water liquid, it can be expected that the HB network in water is disrupted when DMSO is introduced. The RIXS spectra shown in Fig. 11b were obtained upon excitation to the first DMSO resonance,[106] which is energetically situated below the threshold for water excitations. The excited electron is localized and has finite probability to recombine with the core hole, giving rise to the elastic peak at around 533 eV. The excited electron does influence the spectrum, and the final states are neutral excited states rather than ionized as in the XE spectra. Accordingly, additional information is obtained by the combination of RIXS and XES. Indeed, excitation to the two different states contributing to the absorption resonance in the neat liquid (as discussed in the XAS section) leads to quite different RIXS spectra.[14] The variation of the intensity ratio of the two main features upon increasing the excitation energy over the resonance was attributed to a variation of the cross section for scattering over the 15a′ (LUMO) and the 8a″ (LUMO + 1) orbitals. At the lowest excitation energy, the 15a′ scattering channel dominates. Intriguingly, the effects of water mixing seem to be quite small. However, already at the lowest water concentration, in line with the observation in the spectra excited above threshold, the features associated with the 12a′ and 13a′ features are shifted. Again, this can be associated with a weakening of the S–O bond.

The changes in the intensity ratio between the two main peaks are less pronounced in the spectra of the aqueous solution than in pure DMSO and are further attenuated as the water concentration increases. This again indicates a strong water–DMSO interaction and two possible mechanisms have been suggested.[106] A shift of the resonant 8a″ orbital, which has the local S–O π* anti-bonding character, due to the interaction with water is possible. This would reduce the excitation energy dependence in the RIXS spectra as the first resonance would be dominated by the 15a′ channel at all excitation energies. The other possible mechanism is that the reduction of the HOMO related intensity in the high energy part of the structure is similar as discussed for the XE spectra.

The site selectivity of the RIXS technique allows us also to study the HOMOs of molecules and systems, in which the element of interest is contained more than once, like in the carboxyl group (COOH) of acetic acid in aqueous solution. Acetic acid is known to have pH dependent structure and properties and serves as a model system to investigate deprotonation. Horikawa *et al.* compared the emission spectra of a pure aqueous acetic acid solution to one with a pH of 0.29, at which the acetic acid exists mainly in the acid form (COOH), and as well to one with a pH of 11.44, at which the anionic form dominates (COO^-Na^+).[98] They further performed detailed calculations based on the density functional theory (DFT) for an isolated acetate ion.[98] The calculations could reveal the nature of the HOMOs under each emission peak. In a different study regarding glycine's local electronic structure, Gråsjö *et al.*[99] concluded that for the zwitterionic form of glycine, whose carboxylate group is deprotonated similar to the carboxylate group in the study above, the main double peak structure at the energies of 525.5 and 526.6 eV results from the emission of the out-of-plane and in-plane oxygen lone-pair orbitals, respectively. The analysis by Horikawa *et al.*[98] gives more details about the nature of the orbitals by adding a third orbital contributing to these two features. Based on these studies, Golnak *et al.* investigate zinc acetate aqueous solution.[108] RIXS at the oxygen 1s $\rightarrow$ $\pi^*_{C=O}$ absorption resonance of 532.8 eV could give a comprehensive picture about the nature of the HOMOs of the carboxylate group. Interestingly, the HOMO$-$2 peak at 525.2 eV and HOMO$-$3 peak at 522.5 eV have less intensity with respect to their counterparts in the aqueous acetic acid spectrum. Nevertheless, both of them are σ-character orbitals rather than the remaining π-character orbitals. This is the point where the effect of the extra Zn^{2+} ion and water on the local electronic structure of the acetate ion is significant. Actually, the exact nature of the interaction between Na^+ and carboxylate group is not known, nevertheless, it is known that Na^+ is in strong interaction with the carboxylate group.[79] Accordingly, the differences in the RIXS spectra can be attributed to the replacement of Na^+ by Zn^{2+}.

6. X-ray photoelectron spectroscopy

Kai Siegbahn pioneered the electron spectroscopy for chemical analysis (ESCA) which has been developed into an indispensable analytical technique for surface science. The value of this powerful method,[17] which was named later photoelectron spectroscopy (PES) was recognized in the 1981 Nobel Prize awarding in Physics. Nevertheless, the need for high vacuum prohibited PES of volatile liquids and only allowed for investigation of low-vapor-pressure molecules attached to a surface (or close to a surface) or liquid films of low volatility. Siegbahn has introduced in the 1970s liquids to X-rays by using a 0.2 mm beam of liquid formamide.[109–112] In this study, no synchrotron light was used for ionization, but Mg Kα radiation (1253.6 eV). Absolute oxygen 1s, nitrogen 1s and carbon 1s binding energies (BEs) in the liquid phase were assigned. With the invention of the liquid micro-jet technique by Faubel and co-workers,[113] liquids became compatible under high-vacuum conditions, allowing PES investigations.[21,108,114–118] Furthermore, PES from the solid/liquid interface under ambient conditions has been established at the Advanced Light Source of Berkeley lab by Bluhm *et al.*[119] The team contributed significantly to the fundamental understanding of processes in environmental science related to the speciation, distribution, reactivity, transformations, mobility, and potential bioavailability of pollutants and contaminants in the environment. The activities of the PES on interfaces would be beyond the scope of this review, therefore we keep the focus in this section on PES-studies that address ions and molecules in solution using the liquid micro-jet technique. In 2006 Faubel and Winter reviewed the gas-to-liquid PES showing how one can extract valuable information about the MOs *via* the peak shifts (representing MO shifts), peak broadening (hybridization of MOs), and photoionization cross sections.[21] Their review was focusing on photoemission results from aqueous solution systems and surfactants. PES can reveal charge- and site-specific electronic structural information of biomolecules in aqueous solution as well, *e.g.*, for monitoring charge density modifications caused by proton attachment. This has been demonstrated upon changing the pH of an aqueous solution of lysine from basic to acidic, which results in nitrogen 1s and carbon 1s chemical shifts to higher binding energies.[15] Moreover, PE measurements at different pH values reveal a 2.2 eV nitrogen 1s chemical shift toward higher BEs, associated with the protonation of any of the amino groups of aqueous lysine. The sensitivity of photoemission is found to be high enough to distinguish different carbon atoms of lysine in water.

Also the rapid (picoseconds[120]) N–H proton exchange between the two nitrogen atoms of neutral imidazole in water gives rise to distinct binding-energy peaks (chemical shifts) in both, the nitrogen 1s and carbon 1s photoelectron spectra.[121] This example shows that PES is not only highly sensitive to the local atomic environment, but also to its dynamics, which could be down to the fast time scale of the photoelectron emission process (approximately of 10^{-17} s). Gaining information on the picosecond time scale using PES has been extended further by probing the charge-transfer-to-solvent (CTTS) excited states of aqueous chloride *via* the resonant inner-shell photoexcitation of the Cl^-_{aq} 2p level.[118] Halide anions in aqueous solution exhibit intense absorption bands in the deep ultraviolet. These spectral features, which are strongly solvent-dependent, correspond to electron excitation into so-called charge-transfer-to-solvent (CTTS) states. Immediately after excitation the electron is bound in a potential well due to the pre-existing polarization of oriented solvent dipoles around the ion, and obviously no gas-phase analogue exists.[122] The CTTS states have been revealed upon photon excitation of 200 eV to excite these states resonantly from a localized Cl 2p level in aqueous chloride. Combined measurements of photoelectron and Auger-electron spectra from the aqueous chloride solution, when using photon energies near the Cl 2p edge, reveal several empty Cl^-_{aq} levels through the occurrence of so-called spectator Auger decays to double valence-hole states. As the Auger process is extremely fast, *i.e.*, in the order of the Cl 2p lifetime

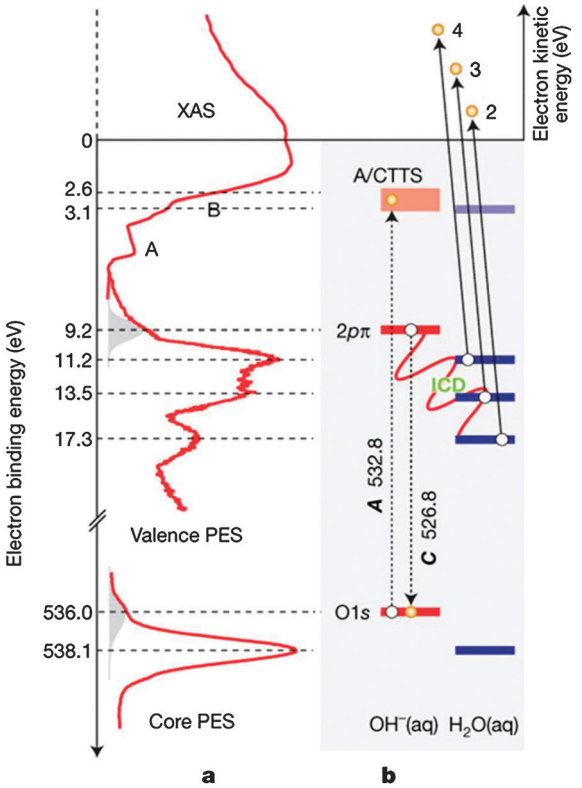

Fig. 12 Energy-level diagram of OH^-(aq) and H_2O(aq). (a) Experimental spectra of a 4 molal NaOH aqueous solution. The H_2O(aq) and OH^-(aq) oxygen 1s photoemission spectra (PES) reveal binding energies of 538.1 and 536.0 eV (grey peak), respectively. The X-ray absorption spectrum (XAS) of OH^-(aq) has a maximum at 532.8 eV. (b) Illustration of ICD for OH^-(aq).[114]

(approximately of 6 fs[123]), the experiment probes CTTS electron dynamics almost at the instant the state is created. The characterization of the CTTS excited state dynamics is an important step forward towards a better understanding of how the solvent responds to the ultrafast movement of charge, which is at the heart of many photon induced processes in aqueous chemistry and biology. The CTTS process is similar to the DCFY which has been discussed in the XAS section of this review and will be further discussed in this section.

Another competitive relaxation mechanism on an ultrafast timescale, which can be probed using PES, is the intermolecular Coulombic decay (ICD) which was observed for OH^- in an aqueous solution.[114] The idea of ICD is based on the transfer of energy from an atom or a molecule to a neighboring atom or a molecule and subsequent ionization of the latter which is ubiquitous in weakly bonded systems.[124] Aziz *et al.* show the detection of this process in aqueous solution which was initiated through core–hole excitation. This gives rise to initial excited states with very short lifetimes that are determined by the lifetime of the core hole and are approximately 4 fs for the oxygen 1s core-level.[114] It is in contrast with the results of the 2p edge excitation of chloride in aqueous solution (presented earlier in this section), where CTTS states have been identified and associated with electron dynamics through the occurrence of spectator Auger-electron peaks. Nevertheless, this phenomenon may be qualitatively different for halide anions[125] than for OH^-[126] given the differences between their hydration patterns. For OH^- aqueous solution, it has been found that resonant excitation of OH^-(aq) does not give rise to local Auger decay even though the excited states of OH^-(aq) are of CTTS nature.[127] Instead, a new and competitive (on an ultrafast timescale) relaxation mechanism, ICD, opens up. Such a process requires favorable orientations and distances between the donor and acceptor molecules, to allow for sufficient orbital overlap yet only negligible rehybridization. It is sufficient that the MO of the initial core–hole vacancy overlaps with the orbital of the resulting final hole at the same molecular site; the second hole has delocalized to a neighboring site.[128] It was argued that the ICD observed in aqueous OH^- supports the idea that the OH^-(aq) is able to donate a hydrogen bond to a neighboring water molecule.[114] Fig. 12 combined the experimental XAS and PES for aqueous OH^- with a schematic presentation of the ICD process. The process is selectively accessing the part of the A-state manifold that corresponds to the short lived OH^-(aq) hydration patterns with donated hydrogen bonds that allow fast ICD.

Another significant contribution of PES has been shown quite recently to the investigation of the radiative and the non-radiative processes at the L-edge of 3d-TMs discussed earlier in this review.[68] In Fig. 13 the processes of X-ray absorption and subsequent photon/electron emission are shown schematically for TMs in solution. Fig. 13a depicts an energy-level scheme illustrating absorption/transmission, *i.e.*, the 2p–3d electron transition at resonant energy (left) and O 1s ionization of H_2O(aq) (right). For Co^{2+} aqueous solution, both processes occur at 776–800 eV photon energy (the L-edge energy range of Co^{2+});

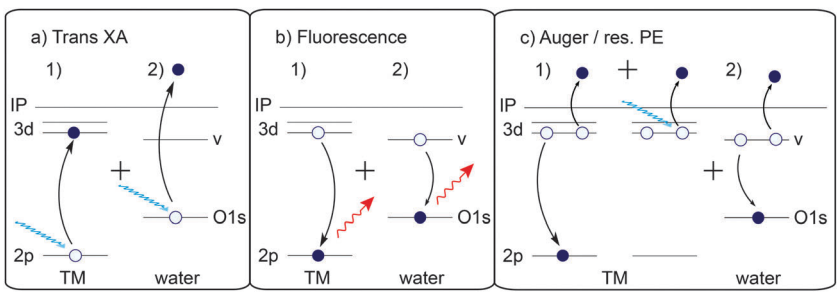

Fig. 13 Illustration of the X-ray absorption process (a) and subsequent fluorescence- (b) and electron-emission (c) decays, occurring in TM-ion aqueous solution at the metal 2p threshold.

the water ionization energy is 538.1 eV.[117] Fig. 13b illustrates the subsequent (~1% minority) fluorescence decay. It shows the refill of the 2p core hole by a 3d electron, with the released energy being carried away by an X-ray photon (left). Analogous processes will occur for H_2O(aq), with the difference though that core refill follows the ionization of water (right). Given the approximately 50 : 1 number-ratio of H_2O molecules to Co^{2+} cations for the concentrations used, the solute fluorescence signal will be measured on top of a broad fluorescence-signal background from water, which contributes at any energy in that range. The latter is due to elastically scattered light emitted by the solvent. As shown in a previous section, a dip, or disappearance of peaks in the TFY-XA spectrum would hence be the net result of solute and solvent contributions, but the relative weights are not trivial to determine. The hybridization between water and metal 3d-MOs, as shown by Aziz *et al.*[66] and quantified using SD-PFY by Soldatov *et al.*,[69] is investigated in a recent PES study by Seidel *et al.*[68] The latter group has shown that such hybridization causes the photo-electron valence signal to be increased considerably as a consequence of the coherent interference of two identical final states. One is reached by direct emission of a photoelectron (direct ionization), and the other results from second-order electron emission, by an Auger-type process. Both processes are indistinguishable (Fig. 13c, left). For completeness, Auger decay for water (Fig. 13c, right) is also presented.

Fig. 14 shows the valence PE spectrum of 0.25 M $CoCl_2$ aqueous solution, recorded at photon energy of 200 eV. The other spectrum, in black, is that from a 0.5 M NaCl aqueous solution (yielding identical chloride concentration), obtained under the same experimental conditions. This comparison is necessary for determining the binding energies (BEs) of the partially occupied metal-derived 3d states because their PE spectrum overlaps with the emission from the 3p orbitals of the Cl^-(aq) counter anion. Subtracting the alkali-halide(aq) spectrum from the $CoCl_2$(aq) spectrum (yielding the difference spectrum, in green) reveals that the lowest ionization of the solution is from the metal complex. This is evidenced by the positive signal at the lowest BEs, extending from 8 eV to 10 eV, well below the onset for ionizing neat liquid water. That signal contains contributions from several 3d-derived Co^{2+}(aq) states which stay unresolved though because of the ~1 eV broad energy distributions from different hydration configurations. In octahedral symmetry, the $3d^7$ level (ground-state configuration of Co^{2+}) splits into e_g (doublet) and t_{2g} (triplet) levels with energy separation defined as 10 Dq. The Co^{2+}(aq) complex is known to assume a high spin ground-state configuration, which is a consequence of the spin-pairing energy being larger than 10 Dq.

The e_g states have a splitting in the energy level which leads to a slight distortion for the octahedral symmetry. In Fig. 14 also the e_g and t_{2g} energies derived from the XA features in Fig. 8a were inserted for comparison. The most important finding from the valence spectrum analysis is that metal t_{2g}-derived levels overlap energetically with the valence band of water, enabling strong orbital mixing, in agreement with previous density-functional theory (DFT) calculations.[2] Accordingly, the strength of the hybridization of MOs in solution between the TM and the ligand can now be experimentally drawn from

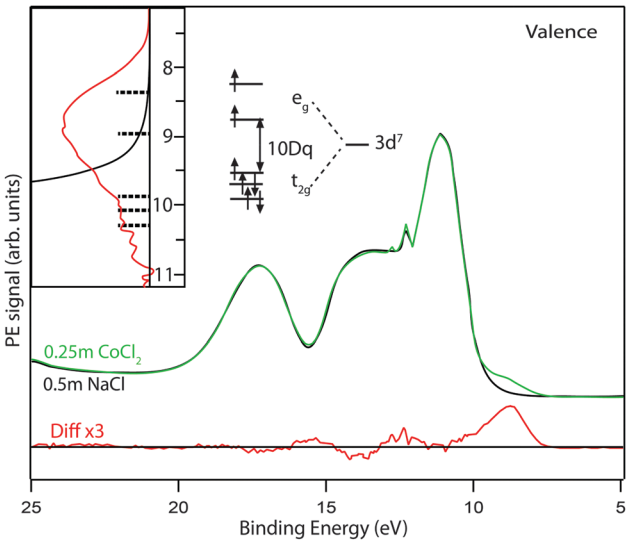

Fig. 14 Off-resonant valence PE spectrum of 0.25 M $CoCl_2$ aqueous solution (in green), measured at 200 eV photon energy. The black spectrum is from 0.5 M NaCl aqueous solution and was measured under the same conditions. The difference spectrum (in red) identifies Co-derived states. Inset: comparison of the experimental low-BE PE peak with the experimental e_g- and t_{2g}-derived states.[68]

the TFY-XAS, PFY-XAS, SD-PFY and PES. Combining all these recently developed/introduced soft X-ray methods in solution adds valuable information about the nature of MOs in solution and electron dynamics that can take place through it.

Many of the previously discussed examples give indirect access to time-resolved processes which could be analyzed if processes could be related to a fast clock (core–hole life-time). Just recently, the emergence of high harmonic light sources, providing short-wavelength radiation in ultrashort light pulses, added the dimension of time to the PES technique and opened the door to (soft) X-ray photoelectron spectroscopy with ultrahigh time resolution.[116] The combination of high harmonic light sources (providing radiation with laser-like beam qualities) and liquid microjet technology recently enabled the first liquid interface PES experiments in the IR/UV-pump and extreme ultraviolet-probe (EUV-probe) configuration. One of the interesting applications of this technique is probing the modification of waters' MOs upon ultrafast heating.[129] If very short infrared laser pulses are used, which are tuned to a strong OH-stretch vibration absorption of water around 3 μm, it is possible to heat the water at a rate faster than the thermal expansion rate and to prepare extreme states of water.[130] These states can have temperatures well above the boiling point, and it has been shown that the water phase may be even heated significantly above the critical temperature.[130] Once water is prepared at these extreme states, it is known that it literally explodes; however, at the sub-picosecond time scale, it moves slowly in time and can thus be resolved with ultrafast spectroscopy. Fig. 15 shows the evolution of the valence MOs of water as a function of time after the ultrafast heating. In the plot, the binding energy is shown against the photoelectron emission counts. The typical valence electron photoemission spectrum of water, in Fig. 15, is correlated to the gas phase emission lines of the $1b_1$,

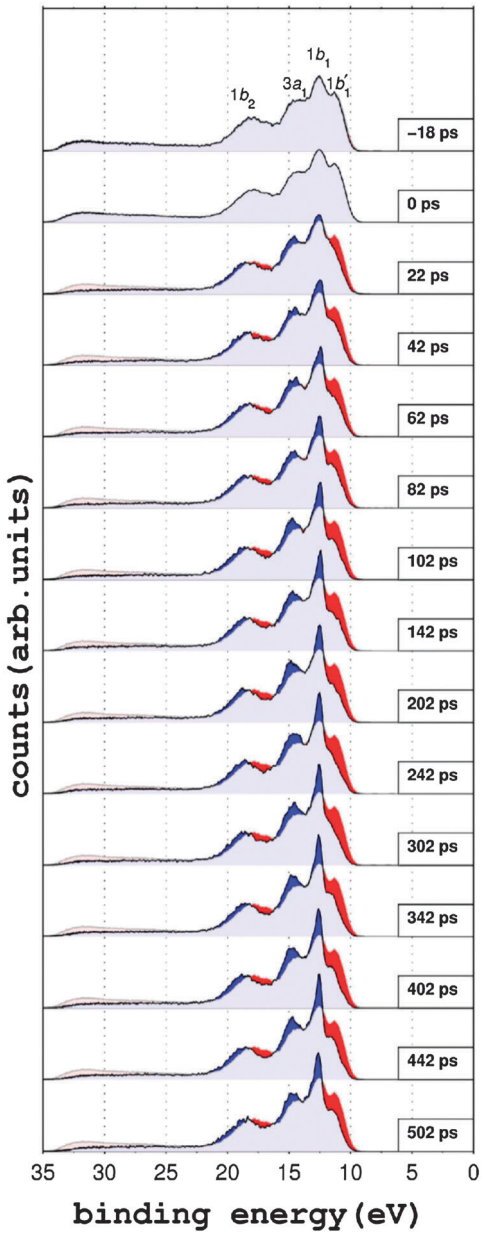

Fig. 15 Time-resolved photoelectron spectra of liquid (before excitation at neg. delay time) and metastable water (excitation at λ_{IR} = 2650 nm).[129,130]

$3a_1$ and $1b_2$ molecular orbitals. The PE signals of the orbitals in the liquid phase are shifted towards lower binding energies with about 1.9 eV. In addition, the liquid peaks show significant broadening and partial overlap. The shifted $1b'_1$ orbital energy peak is clearly visible at the lowest binding energies in the liquid phase. A transition of water from the liquid phase to the gas phase is accompanied by a decrease in intensity in the furthermost shifted $1b'_1$ emission line (color coded in red) of liquid water. At the same time, an increase in intensity is observed for all gas phase lines ($1b_1$, $3a_1$, and $1b_2$) (color coded in blue in Fig. 15).

It is quite obvious that time-resolution has been increased nowadays to a few femtoseconds, and significant efforts are underway to produce stable single attosecond pulses in this spectral range. The quest for higher harmonics and shorter pulses and wavelength will enable the performance of real ultrafast PES experiments in the water window (3–4 nm). Large scale light sources, *e.g.*, LCLS in Stanford, FLASH in Hamburg, and the future European XFEL, will add significant input for investigating a wide range of MO dynamics in solution.

7. Conclusions

Since Robert Mulliken asked the question "What is a molecular orbital?" many scientists have been working on the answer. In the process, modern experimental techniques were developed. In this review, a small fraction of all the work performed is covered and recent contributions of modern soft X-ray synchrotron radiation-based spectroscopy for probing the nature of MOs in solution are presented. The studies of K. Sigbahn and his scientist J. Nordgren, combining electron spectroscopy and X-ray emission on free molecules, have been extended to the liquid phase in the last decade. X-ray absorption has been applied using the iPFY and the SD-PFY techniques, delivering information about unoccupied MOs in the liquid phase. XES and RIXS have been applied on solution and deliver information about the structure and the electron dynamics in the occupied MOs. PES shows its unique power for the investigation of solutions as a complementary method for XAS and XES for revealing the strength of orbital hybridization between solutes and solvents and for time-resolved experiments. Most of the recent studies have been performed on simple molecules, and in the next few years more applied materials will be investigated. Soft X-ray synchrotron light sources and high-harmonic-generation will contribute to the development of such materials. The contributions are expected to be especially significant since it is now possible to investigate the materials under realistic conditions for their function concerning, *e.g.*, temperature and pressure.

Acknowledgements

E. F. A. is thankful for the support by the Helmholtz-Gemeinschaft *via* the young investigator fund VH-NG-635 and the European Research Council grant No. 279344. K. M. L. is thankful for the support by the Helmholtz-Gemeinschaft *via* the Helmholtz Postdoc Programme grant No. PD-059. Parts of this review are discussed in the doctor thesis of Kathrin M. Lange, doctor thesis of Robert Seidel and master thesis of Malte Gotz. Additionally, we thank Nicholas Engel and Kaan Atak for their contributions.

References

1 M. Karelson, V. S. Lobanov and A. R. Katritzky, *Chem. Rev.*, 1996, **96**, 1027.
2 L. Å. Näslund, M. Cavalleri, H. Ogasawara, A. Nilsson, L. G. M. Pettersson, P. Wernet, D. C. Edwards, M. Sandstrom and S. Myneni, *J. Phys. Chem. A*, 2003, **107**, 6869.
3 J. N. Murrell, S. F. Kettle and J. M. Tedder, *The chemical bond*, John Wiley & Sons, Chichester, 1985.

4 K. Osmialowski, J. Halkiewicz, A. Radecki and R. Kaliszan, *J. Chromatogr.*, 1985, **346**, 53.
5 I. Fleming, *Frontier Orbitals and Organic Chemical Reactions*, John Wiley & Sons, New York, 1976.
6 D. F. V. Lewis, C. Ioannides and D. V. Parke, *Xenobiotica*, 1994, **24**, 401.
7 Z. X. Zhou and R. G. Parr, *J. Am. Chem. Soc.*, 1990, **112**, 5720.
8 J. N. Moore, P. A. Hansen and R. M. Hochstrasser, *Proc. Natl. Acad. Sci. U. S. A.*, 1988, **85**, 5062.
9 J. L. Martin, A. Migus, C. Poyart, Y. Lecarpentier, R. Astier and A. Antonetti, *Proc. Natl. Acad. Sci. U. S. A.*, 1983, **80**, 173.
10 M. Lim, T. A. Jackson and P. A. Anfinrud, *Science*, 1995, **269**, 962.
11 Y. Harada, M. Taguchi, Y. Miyajima, T. Tokushima, Y. Horikawa, A. Chainani, Y. Shiro, Y. Senba, H. Ohashi, H. Fukuyama and S. Shin, *J. Phys. Soc. Jpn.*, 2009, **78**, 044802.
12 E. F. Aziz, N. Ottosson, S. Bonhommeau, N. Bergmann, W. Eberhardt and M. Chergui, *Phys. Rev. Lett.*, 2009, **102**, 068103.
13 N. Bergmann, S. Bonhommeau, K. M. Lange, S. M. Greil, S. Eisebitt, F. de Groot, M. Chergui and E. F. Aziz, *Phys. Chem. Chem. Phys.*, 2010, **12**, 4827.
14 K. Atak, N. Engel, K. M. Lange, R. Golnak, M. Gotz, M. Soldatov, J. E. Rubensson, N. Kosugi and E. F. Aziz, *ChemPhysChem*, 2012, **13**, 3106. Fig. 9a is reproduced from this reference with permission. Copyright © 2012 WILEY-VCH Verlag GmbH & Co. KGaA, Weinheim.
15 D. Nolting, E. F. Aziz, N. Ottosson, M. Faubel, I. V. Hertel and B. Winter, *J. Am. Chem. Soc.*, 2007, **129**, 14068.
16 J. Stöhr, *NEXAFS spectroscopy*, Springer-Verlag, Berlin, London, 1992.
17 S. Hüfner, *Photoelectron Spectroscopy: Principles and Applications*, Springer, 2010.
18 F. d. Groot and A. Kotani, *Core level spectroscopy of solids*, CRC Press, Boca Raton, 2008.
19 K. M. Lange and E. F. Aziz, *Chem.–Asian. J.*, 2013, **8**, 318–327.
20 K. M. Lange, E. Suljoti and E. F. Aziz, *J. Electron Spectrosc. Relat. Phenom.*, DOI: 10.1016/j.elspec.2012.09.010.
21 B. Winter and M. Faubel, *Chem. Rev.*, 2006, **106**, 1176.
22 P. A. Brühwiler, O. Karis and N. Martensson, *Rev. Mod. Phys.*, 2002, **74**, 703.
23 H. A. Kramers and W. Heisenberg, *Z. Phys. A: Hadrons Nucl.*, 1925, **31**, 681.
24 F. Gel'mukhanov and H. Ågren, *Phys. Rep.*, 1999, **312**, 87.
25 Y. P. Sun, Q. Miao, A. Mohammed, H. Ågren and F. Gel'mukhanov, *Chem. Phys. Lett.*, 2011, **511**, 16.
26 J. E. Rubensson, J. Luning, S. Eisebitt and W. Eberhardt, *Appl. Phys. A: Mater. Sci. Process.*, 1997, **65**, 91.
27 W. Eberhardt, J. Luning and J. E. Rubensson, *Appl. Phys. A: Mater. Sci. Process.*, 1997, **65**, 89.
28 H. Ågren and F. Gel'mukhanov, *J. Electron Spectrosc. Relat. Phenom.*, 2000, **110**, 153.
29 S. Eisebitt and W. Eberhardt, *J. Electron Spectrosc. Relat. Phenom.*, 2000, **110**, 335.
30 A. Kotani and S. Shin, *Rev. Mod. Phys.*, 2001, **73**, 203.
31 A. Krol, C. S. Lin, Z. H. Ming, C. J. Sher, Y. H. Kao, C. T. Chen, F. Sette, Y. Ma, G. C. Smith, Y. Z. Zhu and D. T. Shaw, *Phys. Rev. B: Condens. Matter Mater. Phys.*, 1990, **42**, 2635.
32 F. de Groot and A. Kotani, *Core level spectroscopy of solids*, CRC Press, Boca Raton, 2008.
33 B. X. Yang and J. Kirz, *Phys. Rev. B: Condens. Matter Mater. Phys.*, 1987, **36**, 1361.
34 S. Schreck, G. Gavrila, C. Weniger and P. Wernet, *Rev. Sci. Instrum.*, 2011, **82**, 103101.
35 M. Freiwald, S. Cramm, W. Eberhardt and S. Eisebitt, *J. Electron Spectrosc. Relat. Phenom.*, 2004, **137**, 413.
36 O. Fuchs, F. Maier, L. Weinhardt, M. Weigand, M. Blum, M. Zharnikovc, J. Denlinger, M. Grunze, C. Heske and E. Umbach, *Nucl. Instrum. Methods Phys. Res., Sect. A*, 2008, **585**, 172.
37 J. Guo, T. Tong, L. Svec, J. Go, C. Dong and J. W. Chiou, *J. Vac. Sci. Technol., A*, 2007, **25**, 1231.
38 T. Tokushima, Y. Harada, O. Takahashi, Y. Senba, H. Ohashi, L. G. M. Pettersson, A. Nilsson and S. Shin, *Chem. Phys. Lett.*, 2008, **460**, 387.
39 T. Tokushima, Y. Harada, Y. Horikawa, O. Takahashi, Y. Senba, H. Ohashi, L. G. M. Pettersson, A. Nilsson and S. Shin, *J. Electron Spectrosc. Relat. Phenom.*, 2010, **177**, 192.
40 O. Fuchs, F. Maier, L. Weinhardt, M. Weigand, M. Blum, M. Zharnikov, J. Denlinger, M. Grunze, C. Heske and E. Umbach, *Nucl. Instrum. Methods Phys. Res., Sect. A*, 2008, **585**, 172.
41 E. F. Aziz, M. Freiwald, S. Eisebitt and W. Eberhardt, *Phys. Rev. B: Condens. Matter Mater. Phys.*, 2006, **73**, 075120.
42 O. Fuchs, L. Weinhardt, M. Blum, M. Weigand, E. Umbach, M. Bär, C. Heske, J. Denlinger, Y. D. Chuang, W. McKinney, Z. Hussain, E. Gullikson, M. Jones, P. Batson, B. Nelles and R. Follath, *Rev. Sci. Instrum.*, 2009, **80**, 063103.
43 M. Nagasaka, T. Hatsui, T. Horigome, Y. Hamamura and N. Kosugi, *J. Electron Spectrosc. Relat. Phenom.*, 2010, **177**, 130.
44 A. Kolmakov, D. A. Dikin, L. J. Cote, J. X. Huang, M. K. Abyaneh, M. Amati, L. Gregoratti, S. Gunther and M. Kiskinova, *Nat. Nanotechnol.*, 2011, **6**, 651.
45 H. Siegbahn and K. Siegbahn, *J. Electron Spectrosc. Relat. Phenom.*, 1973, **2**, 319.
46 M. Faubel, B. Steiner and J. P. Toennies, *J. Chem. Phys.*, 1997, **106**, 9013.
47 K. M. Lange, A. Kothe and E. F. Aziz, *Phys. Chem. Chem. Phys.*, 2012, **14**, 5331.
48 K. M. Lange, R. Könnecke, S. Ghadimi, R. Golnak, M. A. Soldatov, K. F. Hodeck, A. Soldatov and E. F. Aziz, *Chem. Phys.*, 2010, **377**, 1.
49 K. M. Lange, R. Könnecke, M. A. Soldatov, R. Golnak, J.-E. Rubensson, A. Soldatov and E. F. Aziz, *Angew. Chem., Int. Ed.*, 2011, **123**, 10809.
50 K. M. Lange, M. Soldatov, R. Golnak, M. Gotz, N. Engel, R. Könnecke, J. E. Rubensson and E. F. Aziz, *Phys. Rev. B: Condens. Matter Mater. Phys.*, 2012, **85**, 155104.
51 K. R. Wilson, B. S. Rude, T. Catalano, R. D. Schaller, J. G. Tobin, D. T. Co and R. J. Saykally, *J. Phys. Chem. B*, 2001, **105**, 3346.

52 J. L. Dehmer and D. Dill, *Phys. Rev. Lett.*, 1975, **35**, 213.
53 H. Wende, *Rep. Prog. Phys.*, 2004, **67**, 2105.
54 C. Bressler and M. Chergui, *Annu. Rev. Phys. Chem.*, 2010, **61**, 263.
55 G. Hähner, *Chem. Soc. Rev.*, 2006, **35**, 1244.
56 E. F. Aziz, *J. Electron Spectrosc. Relat. Phenom.*, 2010, **177**, 168.
57 E. F. Aziz, *J. Phys. Chem. Lett.*, 2011, **2**, 320.
58 F. M. F. de Groot, M. A. Arrio, P. Sainctavit, C. Cartier and C. T. Chen, *Solid State Commun.*, 1994, **92**, 991.
59 S. Eisebitt, T. Boske, J. E. Rubensson and W. Eberhardt, *Phys. Rev. B: Condens. Matter Mater. Phys.*, 1993, **47**, 14103.
60 Y. Horikawa, H. Arai, T. Tokushima and S. Shin, *Chem. Phys. Lett.*, 2012, **522**, 33.
61 E. F. Aziz, S. Eisebitt, F. de Groot, J. W. Chiou, C. G. Dong, J. H. Guo and W. Eberhardt, *J. Phys. Chem. B*, 2007, **111**, 4440.
62 E. F. Aziz, A. Zimina, M. Freiwald, S. Eisebitt and W. Eberhardt, *J. Chem. Phys.*, 2006, **124**, 114502. Fig. 3 adapted from this reference with permission, Copyright 2006, American Institute of Physics..
63 A. J. Achkar, T. Z. Regier, H. Wadati, Y. J. Kim, H. Zhang and D. G. Hawthorn, *Phys. Rev. B: Condens. Matter Mater. Phys.*, 2011, **83**, 081106.
64 A. J. Achkar, T. Z. Regier, E. J. Monkman, K. M. Shen and D. G. Hawthorn, *Sci. Rep.*, 2011, **1**, 182.
65 M. D. Gotz, M. A. Soldatov, K. M. Lange, N. Engel, R. Golnak, R. Könnecke, K. Atak, W. Eberhardt and E. F. Aziz, *J. Phys. Chem. Lett.*, 2012, **3**, 1619.
66 E. F. Aziz, M. H. Rittmann-Frank, K. M. Lange, S. Bonhommeau and M. Chergui, *Nat. Chem.*, 2010, **2**, 853. Fig. 6 adapted from this reference.
67 M. Bauer, T. Stalinski and E. F. Aziz, *ChemPhysChem*, 2011, **12**, 2088.
68 R. Seidel, S. Ghadimi, K. M. Lange, S. Bonhommeau, M. A. Soldatov, R. Golnak, A. Kothe, R. Könnecke, A. Soldatov, S. Thürmer, B. Winter and E. F. Aziz, *J. Am. Chem. Soc.*, 2012, **134**, 1600. Fig. 14 reprinted from this reference with permission. Copyright 2012 American Chemical Society.
69 M. A. Soldatov, K. M. Lange, M. D. Gotz, N. Engel, R. Golnak, A. Kothe and E. F. Aziz, *Chem. Phys. Lett.*, 2012, **546**, 164. Fig. 8 adapted from this reference page 165, Copyright 2012, with permission from Elsevier.
70 E. F. Aziz, K. M. Lange, S. Bonhommeau and M. Chergui, *Nat. Chem.*, 2012, **4**, 767.
71 K. M. Lange, U. Bergmann, K. F. Hodeck, R. Konnecke, U. Schade and E. F. Aziz, *Phys. Chem. Chem. Phys.*, 2011, **13**, 15423.
72 E. F. Aziz, S. Eisebitt, W. Eberhardt, L. Cwiklik and P. Jungwirth, *J. Phys. Chem. B*, 2008, **112**, 1262.
73 N. Ottosson, E. F. Aziz, H. Bergersen, W. Pokapanich, G. Ohrwall, S. Svensson, W. Eberhardt and O. Bjorneholm, *J. Phys. Chem. B*, 2008, **112**, 16642. Parts of Fig. 4 adapted with permission from this reference. Copyright 2008 American Chemical Society.
74 N. Ottosson, E. F. Aziz, I. L. Bradeanu, S. Legendre, G. Ohrwall, S. Svensson, O. Bjorneholm and W. Eberhardt, *Chem. Phys. Lett.*, 2008, **460**, 540. Parts of Fig. 4 adapted from this reference, Copyright 2008, with permission from Elsevier.
75 Y. Jugnet, F. J. Himpsel, P. Avouris and E. E. Koch, *Phys. Rev. Lett.*, 1984, **53**, 198.
76 A. P. Hitchcock and C. E. Brion, *J. Electron Spectrosc. Relat. Phenom.*, 1980, **19**, 231.
77 K. H. Sze, C. E. Brion, M. Tronc, S. Bodeur and A. P. Hitchcock, *Chem. Phys.*, 1988, **121**, 279.
78 T. Clark, J. S. Murray, P. Lane and P. Politzer, *J. Mol. Model.*, 2008, **14**, 689.
79 E. F. Aziz, N. Ottosson, S. Eisebitt, W. Eberhardt, B. Jagoda-Cwiklik, R. Vacha, P. Jungwirth and B. Winter, *J. Phys. Chem. B*, 2008, **112**, 12567. Parts of Fig. 4 adapted from this reference with permission. Copyright 2008 American Chemical Society.
80 S. Bonhommeau, N. Ottosson, W. Pokapanich, S. Svensson, W. Eberhardt, O. Bjorneholm and E. F. Aziz, *J. Phys. Chem. B*, 2008, **112**, 12571.
81 I. Alperovich, D. Moonshiram, A. Soldatov and Y. Pushkar, *Solid State Commun.*, 2012, **152**, 1880.
82 G. Fronzoni, R. Francesco, M. Stener and M. Causa, *J. Phys. Chem. B*, 2006, **110**, 9899.
83 G. Fronzoni, M. Stener, P. Decleva, F. Wang, T. Ziegler, E. van Lenthe and E. J. Baerends, *Chem. Phys. Lett.*, 2005, **416**, 56.
84 B. T. Thole, G. Vanderlaan, J. C. Fuggle, G. A. Sawatzky, R. C. Karnatak and J. M. Esteva, *Phys. Rev. B: Condens. Matter Mater. Phys.*, 1985, **32**, 5107.
85 R. K. Hocking, E. C. Wasinger, Y. L. Yan, F. M. F. deGroot, F. A. Walker, K. O. Hodgson, B. Hedman and E. I. Solomon, *J. Am. Chem. Soc.*, 2007, **129**, 113.
86 K. M. Lange, R. Golnak, S. Bonhommeau and E. F. Aziz, *Chem. Commun.*, 2013, **49**, 4163–4165.
87 F. M. F. de Groot, *Nat. Chem.*, 2012, **4**, 766.
88 T. Z. Regier, A. J. Achkar, D. Peak, J. S. Tse and D. G. Hawthorn, *Nat. Chem.*, 2012, **4**, 765.
89 A. J. Achkar, T. Z. Regier, H. Wadati, Y. J. Kim, H. Zhang and D. G. Hawthorn, *Phys. Rev. B: Condens. Matter Mater. Phys.*, 2011, **83**, 129901.
90 M. D. Gotz, M. A. Soldatov, K. M. Lange, N. Engel, R. Golnak, R. Konnecke, K. Atak, W. Eberhardt and E. F. Aziz, *J. Phys. Chem. Lett.*, 2012, **3**, 1619. Fig. 7 is adapted from this reference with permission. Copyright 2012 American Chemical Society.
91 K. M. Lange, R. Könnecke, M. Soldatov, R. Golnak, J. E. Rubensson, A. Soldatov and E. F. Aziz, *Angew. Chem., Int. Ed.*, 2011, **50**, 10621.
92 D. T. Richens, *The Chemistry of Aqua Ions: Synthesis, Structure and Reactivity: A Tour Through the Periodic Table of the Elements*, Wiley, New York, 1st edn, 1997.
93 J. Nordgren, H. Ågren, L. Selander, C. Nordling and K. Siegbahn, *Phys. Scr.*, 1977, **16**, 280.
94 J. Nordgren and J. H. Guo, *J. Electron Spectrosc. Relat. Phenom.*, 2000, **110**, 1.

95 G. Ghiringhelli, A. Piazzalunga, C. Dallera, G. Trezzi, L. Braicovich, T. Schmitt, V. N. Strocov, R. Betemps, L. Patthey, X. Wang and M. Grioni, *Rev. Sci. Instrum.*, 2006, **77**, 113108.
96 T. Tokushima, Y. Harada, H. Ohashi, Y. Senba and S. Shin, *Rev. Sci. Instrum.*, 2006, **77**, 063107.
97 T. Tokushima, Y. Horikawa, Y. Harada, O. Takahashi, A. Hiraya and S. Shin, *Phys. Chem. Chem. Phys.*, 2009, **11**, 1679.
98 Y. Horikawa, T. Tokushima, Y. Harada, O. Takahashi, A. Chainani, Y. Senba, H. Ohashi, A. Hiraya and S. Shin, *Phys. Chem. Chem. Phys.*, 2009, **11**, 8676.
99 J. Grasjo, E. Andersson, J. Forsberg, L. Duda, E. Henke, W. Pokapanich, O. Bjorneholm, J. Andersson, A. Pietzsch, F. Hennies and J. E. Rubensson, *J. Phys. Chem. B*, 2009, **113**, 16002.
100 Y. Horikawa, T. Tokushima, A. Hiraya and S. Shin, *Phys. Chem. Chem. Phys.*, 2010, **12**, 9165.
101 J. H. Guo, Y. Luo, A. Augustsson, J. E. Rubensson, C. Såthe, H. Ågren, H. Siegbahn and J. Nordgren, *Phys. Rev. Lett.*, 2002, **89**, 137402.
102 A. Nilsson and L. G. M. Pettersson, *Chem. Phys.*, 2011, **389**, 1.
103 Y. P. Sun, F. Hennies, A. Pietzsch, B. Kennedy, T. Schmitt, V. N. Strocov, J. Andersson, M. Berglund, J. E. Rubensson, K. Aidas, F. Gel'mukhanov, M. Odelius and A. Foehlisch, *Phys. Rev. B: Condens. Matter Mater. Phys.*, 2011, **84**, 132202. Reprinted Fig. 10 and parts of Fig. 9 from this reference with permission. Copyright 2011 by the American Physical Society.
104 Y. Zheng, J. J. Neville, C. E. Brion, Y. Wang and E. R. Davidson, *Chem. Phys.*, 1994, **188**, 109.
105 R. G. Pearson, *J. Org. Chem.*, 1989, **54**, 1423.
106 N. Engel, K. Atak, K. M. Lange, M. Gotz, M. Soldatov, R. Golnak, E. Suljoti, J.-E. Rubensson and E. F. Aziz, *J. Phys. Chem. Lett.*, 2012, **3**, 3697. Fig. 11 is adapted from this reference with permission. Copyright 2012 American Chemical Society.
107 K. M. Lange, M. Soldatov, R. Golnak, M. Gotz, N. Engel, R. Könnecke, J.-E. Rubensson and E. F. Aziz, *Phys. Rev. B: Condens. Matter Mater. Phys.*, 2012, **85**, 155104.
108 R. Golnak, K. Atak, E. Suljoti, K. F. Hodeck, K. M. Lange, M. A. Soldatov, N. Engel and E. F. Aziz, *Phys. Chem. Chem. Phys.*, 2013, **15**, 8046–8049.
109 B. Lindberg, L. Asplund, H. Fellnerfeldegg, P. Kelfve, H. Siegbahn and K. Siegbahn, *Chem. Phys. Lett.*, 1976, **39**, 8.
110 H. Siegbahn, L. Asplund, P. Kelfve and K. Siegbahn, *J. Electron Spectrosc. Relat. Phenom.*, 1975, **7**, 411.
111 H. Fellnerfeldegg, H. Siegbahn, L. Asplund, P. Kelfve and K. Siegbahn, *J. Electron Spectrosc. Relat. Phenom.*, 1975, **7**, 421.
112 H. Siegbahn, L. Asplund, P. Kelfve, K. Hamrin, L. Karlsson and K. Siegbahn, *J. Electron Spectrosc. Relat. Phenom.*, 1974, **5**, 1059.
113 R. E. Grisenti, R. A. C. Fraga, N. Petridis, R. Dorner and J. Deppe, *Europhys. Lett.*, 2006, **73**, 540.
114 E. F. Aziz, N. Ottosson, M. Faubel, I. V. Hertel and B. Winter, *Nature*, 2008, **455**, 89. Fig. 12 reprinted from this reference by permission from Macmillan Publishers Ltd: Nature, Copyright: 2008.
115 B. Winter, R. Weber, W. Widdra, M. Dittmar, M. Faubel and I. V. Hertel, *J. Phys. Chem. A*, 2004, **108**, 2625.
116 M. Faubel, K. R. Siefermann, Y. Liu and B. Abel, *Acc. Chem. Res.*, 2012, **45**, 120.
117 B. Winter, E. F. Aziz, U. Hergenhahn, M. Faubel and I. V. Hertel, *J. Chem. Phys.*, 2007, **126**, 124504.
118 B. Winter, E. F. Aziz, N. Ottosson, M. Faubel, N. Kosugi and I. V. Hertel, *J. Am. Chem. Soc.*, 2008, **130**, 7130.
119 H. Bluhm, K. Andersson, T. Araki, K. Benzerara, G. E. Brown, J. J. Dynes, S. Ghosal, M. K. Gilles, H. C. Hansen, J. C. Hemminger, A. P. Hitchcock, G. Ketteler, A. L. D. Kilcoyne, E. Kneedler, J. R. Lawrence, G. G. Leppard, J. Majzlan, B. S. Mun, S. C. B. Myneni, A. Nilsson, H. Ogasawara, D. F. Ogletree, K. Pecher, M. Salmeron, D. K. Shuh, B. Tonner, T. Tyliszczak, T. Warwick and T. H. Yoon, *J. Electron Spectrosc. Relat. Phenom.*, 2006, **150**, 86.
120 W. Munch, K. D. Kreuer, W. Silvestri, J. Maier and G. Seifert, *Solid State Ionics*, 2001, **145**, 437.
121 D. Nolting, N. Ottosson, M. Faubel, I. V. Hertel and B. Winter, *J. Am. Chem. Soc.*, 2008, **130**, 8150.
122 F. H. Long, H. Lu, X. L. Shi and K. B. Eisenthal, *Chem. Phys. Lett.*, 1990, **169**, 165.
123 R. F. Fink, M. Kivilompolo, H. Aksela and S. Aksela, *Phys. Rev. A*, 1998, **58**, 1988.
124 X. Y. Chen and S. E. Bradforth, *Annu. Rev. Phys. Chem.*, 2008, **59**, 203.
125 M. J. Blandamer and M. F. Fox, *Chem. Rev.*, 1970, **70**, 59.
126 R. A. Crowell, R. Lian, I. A. Shkrob, D. M. Bartels, X. Y. Chen and S. E. Bradforth, *J. Chem. Phys.*, 2004, **120**, 11712.
127 M. Fox and R. Mcintyre, *Faraday Discuss.*, 1977, **64**, 167.
128 L. S. Cederbaum, J. Zobeley and F. Tarantelli, *Phys. Rev. Lett.*, 1997, **79**, 4778.
129 O. Link, E. Vohringer-Martinez, E. Lugovoj, Y. X. Liu, K. Siefermann, M. Faubel, H. Grubmuller, R. B. Gerber, Y. Miller and B. Abel, *Faraday Discuss.*, 2009, **141**, 67.
130 O. Link, E. Lugovoy, K. Siefermann, Y. Liu, M. Faubel and B. Abel, *Appl. Phys. A: Mater. Sci. Process.*, 2009, **96**, 117. Fig. 15 was reproduced from this reference with kind permission of Springer Science+Business Media.